

CSIRO Intelligent Grid Research Cluster- Project 7

Microgrid Operation and Control

**Manjula Dewadasa
Arindam Ghosh
Gerard Ledwich**

DELIVERABLE 5: Switching Control strategies for Distributed Generation

Executive Summary

A microgrid can be considered as a small grid based on distributed generators (DGs). The microgrid can operate either in grid connected or islanded (i.e., autonomous) mode. The available power of all DG units should meet the total load demand for autonomous operation; otherwise load shedding need to be implemented. The frequency and voltage in an autonomous microgrid should be maintained within the predefined limits.

The DGs in a microgrid can be classified as either, dispatchable and nondispatchable, or inertial and non-inertial depending on their power flow control and dynamic behavior. The output power of dispatchable DGs such as microturbines, fuel cells and bio-diesel generators are controlled to maintain the desired system frequency and voltage in an autonomous microgrid. On the other hand, nondispatchable DGs such as wind and PV, in which the output power depends on the environmental conditions, are controlled in maximum power point tracking (MPPT) to harness as much energy as possible.

The dynamic response of inertial and non-inertial DGs is different. The response of inertial DGs (rotary machine based) will be slower compared to the non-inertial DGs (converter interfaced). For example, a diesel generator and a hydro generator are inertial sources since they include synchronous generators with their rotating inertial masses. Thus, a finite time is required to change output power of an inertial DG. On the other hand, the DGs connected through converters such as PVs, fuel cells and batteries are non-inertial and they can respond to change real and reactive power output very quickly. This mismatch in response rate can create power and frequency fluctuations in an autonomous microgrid where no single dominant energy source is present. Therefore, the control and power management strategies are vital for an autonomous microgrid in the presence of few different types of DGs.

The purpose of this report is to investigate the interaction of different types of DGs during synchronization, dynamic power sharing and load changes to identify the issues and propose better control strategies for a stable operation of a microgrid operating in autonomous mode. Decentralized control of DGs and load power sharing using frequency and voltage droop control are considered. It has been assumed that no explicit communication system is present. Modified droop control strategies are proposed to improve the performance of the existing droop control methods. Investigations are performed to improve the plug and play approach for different types of DGs to minimize any transient oscillation and thereby improving the system stability.

The modeling of a diesel generator, a doubly fed induction generator (DFIG), a solar PV, a fuel cell and a battery storage is performed in PSCAD for simulation studies. The frequency and voltage droop controls are used to regulate the system frequency and voltage in the autonomous microgrid and share the real and reactive power requirement of loads amongst dispatchable DGs. In the droop control, the real and reactive power output of each DG in the microgrid is controlled. Each DG in the system uses its real power output to set the frequency at its point of connection (PC) while the reactive power output to set the PC voltage magnitude. The Non-dispatchable DGs are controlled in MPPT.

The interaction between different types of DGs is considered in the simulation. As the first step, synchronization of inertial DGs to an autonomous microgrid containing inertial DGs only is investigated. Two diesel generators are considered for the study. In this case, the

transient oscillations in real power and frequency are observed during DG synchronization. These oscillations are observed due to the slower governor response of the inertial DG. The output speed/frequency of each inertial DG cannot be changed instantly according to the value requested from the frequency droop. The absence of a single strong source (such as utility grid) in an autonomous microgrid, these frequency oscillations manifest more vigorously. Moreover, the two diesel generators are separated by a small line segment, which further limit the damping. Therefore, to minimize these transient oscillations, a method is proposed to achieve a smooth droop transfer characteristic for the incoming inertial DG. The proposed droop is obtained by slowly changing the frequency setting of incoming generator from the PC frequency to the droop frequency with an appropriate time constant.

As the second step, the interaction between non-inertial DGs which are connected through converters is investigated. It is shown that the response is smooth during synchronization and load change due to the fast response of the converters. The system steady state is attained very quickly.

Next, the response of a hybrid microgrid containing an inertial DG and a non-inertial DG is investigated. It is observed that there are frequency and real power fluctuations during DG and load connections. Since the inertial DG responds slowly, the real power output cannot increase quickly and the system takes finite time period to reach the steady state. Therefore, the slower response of inertial DG initiates frequency and real power fluctuations in the autonomous microgrid. To minimize the transient oscillations in the presence of both inertial and non-inertial sources, a method called *integral to droop line* is proposed. This is only implemented on the non-inertial DGs in the microgrid. In the proposed droop control, the frequency droop is modified by introducing an integration process to reach the steady state frequency droop point in the system. The error between calculated droop frequency and the frequency at PC is passed through an integrator to force the operating frequency of the DG to reach the steady state droop point within a defined time period. It is shown that the proposed integral to droop line has the ability to improve the dynamic power sharing amongst inertial and non-inertial DGs avoiding transient oscillations. Also, it ensures the proper load power sharing amongst the DGs.

The microgrid control and power management with dispatchable, non-dispatchable, inertial and non-inertial DGs are studied next with the proposed droop control strategies. The key findings show the improved performance of the microgrid with the use of proposed control strategies. Then, power management and control strategies required to incorporate dispatchable DGs, non-dispatchable DGs and battery storage (BS) are discussed. An intelligent control system (ICS) for the BS is proposed to manage the charging and discharging while maintaining the operating reserve in the BS to achieve system stability. To enhance a flexible operation in the microgrid maximizing the benefits of renewable energy, a control strategy based on adaptive droop is proposed for the BS. During the charging and discharging, the slope of the droop is selected appropriately by the ICS considering several constraints.

In this report, new control strategies are proposed to improve the transient behavior and dynamic load power sharing in an autonomous microgrid. The results show that the proposed control and power management strategies have the ability to further improve the microgrid performance.

1. Introduction

A microgrid can be considered as a small grid based on distributed generators (DGs). Generally, the microgrid consists of renewable energy based DGs and combined heat and power plants. It can supply power to small/medium sized urban housing communities or to large rural areas. It can be an economical, environment friendly and reliable way to supply power at distribution levels. The sources in a microgrid can be mainly classified as dispatchable or nondispatchable in terms of power flow control [1,2]. The output power of dispatchable sources such as microturbines, fuel cells and bio-diesel generators can be controlled to maintain the desired system frequency and voltage in an isolated microgrid. However, nondispatchable sources such as wind and PV, in which the output power depends on the environmental conditions, are expected to be mainly controlled on the basis of maximum power point tracking (MPPT).

The sources in a microgrid can also be classified as inertial and non-inertial depending on the way they are connected to the system. For example, a diesel generator and a hydro generator are inertial sources since they include synchronous generators with their rotating inertial masses. On the other hand, the sources connected through converters such as PV, fuel cell and batteries are non-inertial since power output through these DGs can be changed instantaneously. A microgrid can operate either in grid connected or islanded mode. The available power of all DG units should meet the total load demand for islanded operation; otherwise load shedding need to be implemented. The control of real and reactive power output of the sources is essential to maintain a stable operation in a microgrid, especially when it operates in the islanded mode. The frequency and voltage in an islanded (autonomous) microgrid should be maintained within predefined limits. The frequency variations are very small in strong grids; however, large variations can occur in autonomous grids [3]. Thus power management strategies are vital for an autonomous microgrid in the presence of few small DG units, where no single dominant energy source is present to supply the energy requirement [4]. Also, fast and flexible power control strategies are necessary to damp out transient power oscillations in an autonomous microgrid where no infinite source available [5].

Many researchers have addressed the operational, control and protection issues in microgrids [2, 6-9]. The real and reactive power output of a generator can be independently controlled by changing the voltage angle (based on frequency) and the magnitude respectively [10-11]. Therefore, frequency and voltage droop controls are the most common methods used to share the real and reactive load power in a microgrid. However, the reactive power sharing among the DGs will not be precise as expected from the droop due to microgrid cable impedances [12].

Different droop controls and converter control strategies have been proposed. The control strategies required for converter connected islanded microgrid system is analyzed in [12]. A droop control based on the active and reactive current control is presented for parallel converters [10]. The control of parallel converters in a standalone ac power supply without the need of communication is presented in [13]. The response of microgrid in the presence of a diesel generator and a converter interfaced DG has been investigated in [14]. The control of parallel converters for load sharing in a microgrid operated in both grid connected and islanded mode is presented [15]. In [16], droop based on angle is proposed to share the real power in a converter connected microgrid.

The literature survey reveals that the most researchers have only considered the control of converter connected microgrids. Little attention has been given so far to the control and operational aspects of hybrid microgrids, which consist of both inertial and non-inertial sources. The purpose of this report is to analyze the interaction of different types of sources during dynamic power sharing to propose better control strategies in an autonomous microgrid. Also, the control and power management strategies are proposed in the presence of both dispatchable and non-dispatchable sources in an autonomous microgrid. Decentralized control of DGs, DG synchronization and load power sharing using frequency and voltage droop controllers are considered in this report. Modified droop control strategies are proposed to improve the existing droop control methods to minimize the transient oscillations. It has been assumed that no explicit communication system is present. Investigations are performed to improve the plug and play approach for different types of microgrid sources to minimize any transient oscillation and thereby improving the system stability.

2. Real and Reactive Power Sharing in a Microgrid

As mentioned before, both inertial and non-inertial sources can be present in a hybrid microgrid. These different types of sources can connect or disconnect to the network at any time. However, the dynamic behavior of inertial and non-inertial sources is different. Microsources such as solar photovoltaic (PV) and fuel cell produce power at dc voltage. Therefore, voltage source converters (VSCs) are required to convert dc voltage into ac voltage. These DGs connected through converters can respond very quickly to changes in real and reactive power demands. On the other hand, the response of a synchronous machine based DGs will be much slower.

Non-dispatchable sources such as solar and wind may not be available all the time. However, when they are available, it is better to harness as much power as possible by controlling them through MPPT. However at the same time, dispatchable sources may also be connected to an autonomous microgrid. Therefore, the power management and dynamic interaction must be investigated. Consider the schematic diagram of the proposed QUT microgrid as shown in Fig. 1. This contains a diesel generator, a PV array, a fuel cell, a battery storage unit and a doubly fed induction generator (DFIG) along with loads. We shall study the behavior of this microgrid during generator synchronization and load changes in order to have a stable microgrid operation.

2.1. Droop Control

In a conventional frequency droop control method, each DG in the system uses its real power output to set the frequency at its point of connection (PC). Thus, the system frequency will act as the communication signal amongst the DGs to share the real power appropriately. The conventional frequency droop characteristic can be expressed as [10, 13, 17],

$$f^* = f_r + m \times (0.5P_r - P^*) \quad (1)$$

where f^* is the instantaneous frequency setting for the DG considered, f_r is the rated frequency of the system, P_r is the rated real power output of the DG and P^* is the measured actual real power output of the DG. The droop coefficient is denoted by m . The frequency droop characteristic in (1) is shown in Fig. 2. In this figure, isochronous frequency range is denoted using the allowable minimum and maximum system frequency (i.e., f_{min} and f_{max}

respectively). When a DG operates in frequency droop control mode, the system frequency can change between f_{min} and f_{max} depending on the value of real power output. A slower outer control loop can be used to shift the droop line vertically by changing the rated frequency to restore the steady state frequency to the nominal value (i.e., load frequency control).

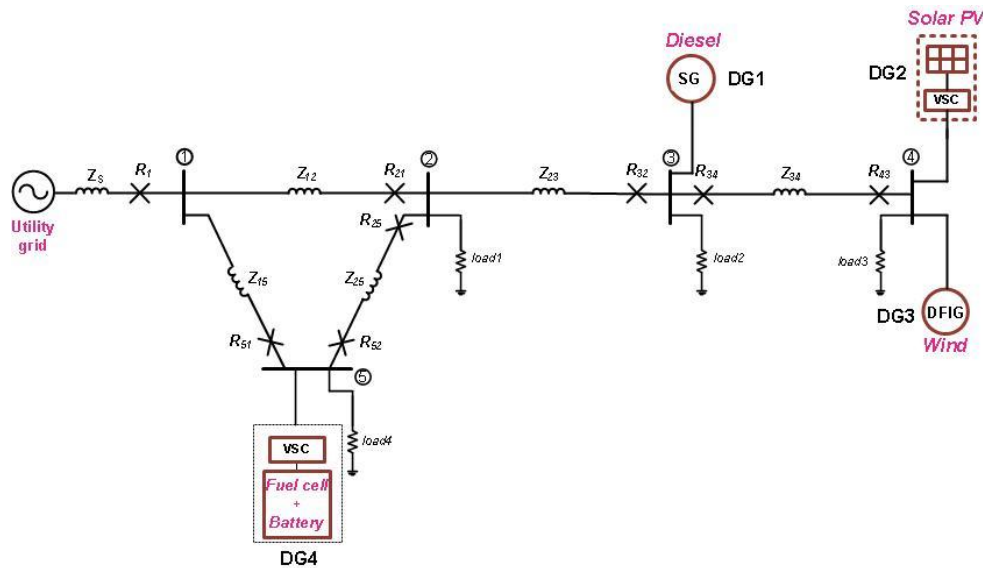


Fig. 1 Schematic diagram of the QUT microgrid.

The droop coefficient m can be calculated using defined values of minimum and maximum frequency and the rated real power output of the DG. When few DGs with different capacities are operating in the frequency droop control, each generator may have a unique value for the droop coefficient, m . The different droop coefficients allow sharing the total load power requirement among the DGs according to a predefined ratio. For example, the total load power requirement of a microgrid can be shared proportional to rated real power output of each DG.

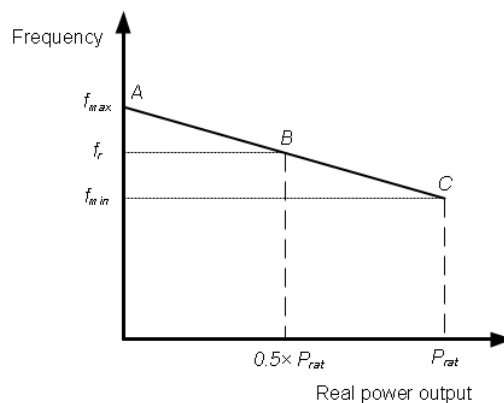


Fig. 2. Frequency droop characteristic of a generator.

The output voltage magnitude of a DG can be controlled to change the reactive power supplied to a system. However, in the presence of a number of DGs, maintaining a voltage to a pre-defined value can cause the reactive power circulation amongst these DGs. This becomes more prevalent when the microgrid has short line segments. This problem can be minimized by implementing voltage droop control in all the DGs. Also, the voltage droop

control results in reactive load power sharing in the microgrid. The conventional voltage droop control characteristic can be given by [10, 13],

$$V^* = V_r + n \times (0.5Q_r - Q^*) \quad (2)$$

where V^* is the instantaneous voltage magnitude setting for the DG, V_r is the rated voltage of the microgrid system, Q_r is the rated reactive power output of the DG and Q^* is the measured actual reactive power output. The voltage droop coefficient is denoted by n . The voltage droop characteristic given in (2) is shown in Fig. 3. In this figure, the minimum and maximum allowable voltages in the system are represented by V_{min} and V_{max} respectively. The voltage droop coefficient can be calculated using the rated reactive power output of the DG and the minimum and maximum voltage levels.

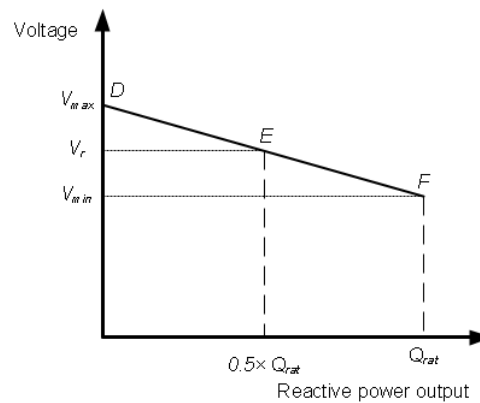


Fig. 3. Voltage droop characteristic of a generator.

The frequency and voltage droop controls in (1) and (2) are employed in each dispatchable DG to maintain the microgrid frequency and voltage within the specified standards. It also results in proper power sharing in the microgrid. Moreover, as mentioned earlier, the non-dispatchable DGs in the microgrid are operated in MPPT mode. In this report, the interaction between different types of DGs is investigated considering transient response and dynamic load power sharing in an autonomous microgrid. It is assumed that the microgrid can consist of only inertial sources or only non-inertial sources or both. The synchronization of DGs into the microgrid is also considered in the analysis.

3. A Simple Microgrid Operation Study

Method

The schematic diagram of the system under study is shown in Fig. 4, while system data are listed in Table 1. In this system, two DGs, DG1 and DG2 are connected at BUS-1 and BUS-3 respectively. The real and reactive power output of DG1 and DG2 are denoted by P_1 , Q_1 and P_2 , Q_2 respectively. The DG circuit breakers are used for synchronization and isolation purposes. Two loads, *load1* and *load2* are connected at BUS-2 and BUS-4. It is to be noted that each DG and load in the microgrid are connected through a short line segment. The microgrid is modeled in PSCAD for simulation.

Different types of DG combinations are considered in the microgrid simulation. The frequency and voltage droops are employed to control and share the real and reactive power output of each dispatchable DG in the microgrid. Depending on the loading condition, the

droop controller will calculate the operating frequency for each DG. The droop coefficients for each DG are selected to control the frequency within isochronous frequency range of ± 0.25 Hz. The voltage limits are set be within the $\pm 6\%$ of nominal value while sharing the real and reactive power amongst loads proportional to the DG power rating.

It is to be noted that the primary aim of this study is to investigate the transient behavior of sources in a microgrid. Therefore no attempt has been made to restore the frequency to the nominal value by shifting droop line vertically using a slower control loop. Different case studies are considered. They are discussed below.

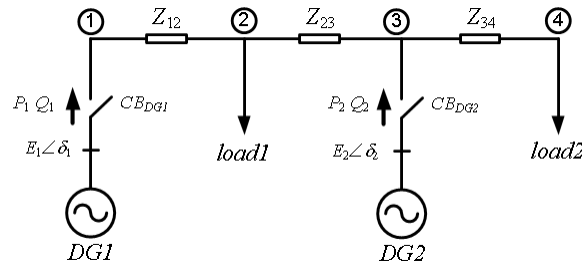


Fig. 4. Schematic diagram of two DGs sharing loads.

TABLE 1: PARAMETERS OF THE SYSTEM OF FIG. 4.

System data	Value
System frequency	50 Hz
System voltage	0.415 kV rms (L-L)
DG1 power rating	(12 + j 8) kVA
DG2 power rating	(15 + j 10) kVA
Feeder impedance ($Z_{12}=Z_{23}$)	(0.025 + j 1.2566) Ω
<i>load1</i> impedance	(15 + j 11.781) Ω
<i>load2</i> impedance	(20 + j 15.708) Ω
Frequency droop coefficient (Hz/kW)	
DG1	m1=0.0417
DG2	m2=0.0333
Voltage droop coefficient (V/kvar)	
DG1	n1=1.2
DG2	n2=1.5

3.1. Microgrid Operation with Inertial DGs

In this study, it has been assumed that microgrid only contains dispatchable inertial DGs, in which both the DGs are assumed to be diesel generators. The diesel generator modeling and its parameters are presented in Appendix A. Each generator consists of an internal combustion (IC) engine coupled to a synchronous generator. The IC engine is integrated with a governor for controlling the output speed of the engine shaft by adjusting the amount of fuel supplied to the engine. Once the frequency droop of the diesel generator is activated, the IC engine maintains the required output shaft speed to a value requested by the droop. Also the diesel generator is incorporated with an exciter and a voltage regulator to control the output terminal voltage. The required value for the regulated voltage can be set based on the voltage droop.

The real and reactive load power sharing amongst diesel generators and synchronization of generators are investigated. To analyze the generator synchronization, it is assumed that DG1 is connected to the system supplying both *load1* and *load2*, while the

microgrid is operating in autonomous mode. Before DG2 can be synchronized to the microgrid, the voltage magnitude of incoming generator (i.e. DG2) is adjusted to the value equal to the PC voltage. Then the phase angle of DG2 and the frequency are adjusted to match the values at PC. Thereafter, CB_{DG2} is closed at the point of voltage zero crossing. In the simulation, DG2 is connected to the microgrid at 26.593 s once the synchronization conditions are satisfied. After the DG2 is connected, both DGs operate in frequency and voltage droop sharing the load power in the microgrid.

The real and reactive power sharing before and after the connection of DG2 is shown in Fig. 5Fig. . It can be seen that DG2 starts supplying the real and reactive power after the synchronization. The variation of DG frequency setting based on droop (i.e. the frequency calculated from the droop equation) is shown in Fig. 6Fig. . Just before the synchronization, DG1 maintains the microgrid frequency in droop control and the frequency of DG2 is adjusted to the PC frequency (i.e. equal to DG1 droop frequency) for synchronization purpose. However, once the DG2 is connected, its frequency changes to no load frequency since real power output is zero at the moment of connection. Subsequently, DG2 starts injecting real power causing droop frequency to decrease gradually. On the other hand, the real power output of DG1 gradually decreases as DG2 injects more power to the microgrid. The system comes to the steady state after about 12 s. The droop coefficients, given in Table 1, are selected to supply the load power proportional to the DG capacity. In accordance with the ratio of real power ratings of these two DGs given in Table 1, the ratio of real power output between two DGs is 1.25. The output currents of DG1 and DG2 during and after the synchronization are shown in Fig. 7.

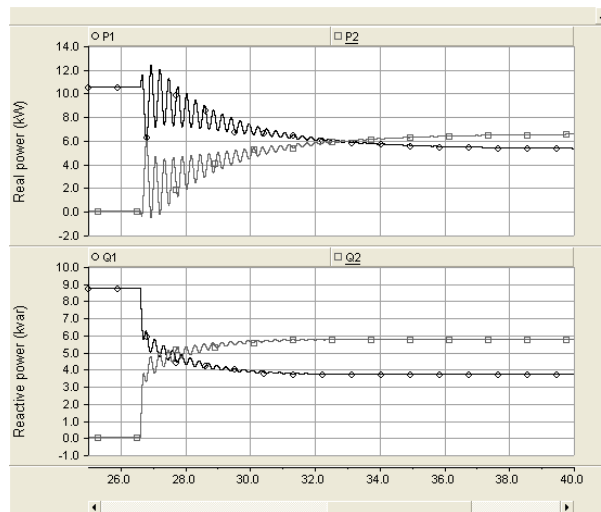


Fig. 5. Real and reactive power sharing amongst inertial DGs.

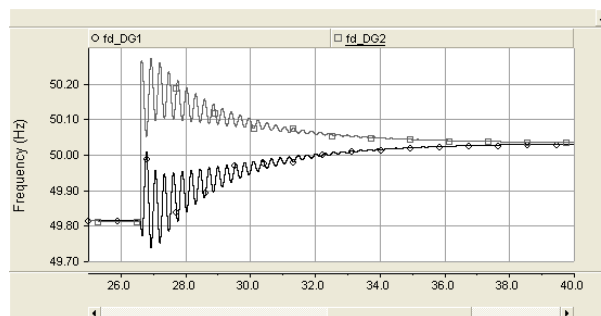


Fig. 6. The variation of DG droop frequencies of inertial DGs.

From Figs. 5 and 6, transient oscillations can be seen in frequency and real power waveforms after DG2 is connected to the microgrid. The system oscillations are further demonstrated by the DG output currents shown in Fig. 7. The two DGs inject currents at slightly different frequencies until the steady state droop point is achieved. The main reason for these oscillations is the slower governor response of these inertial generators. The output speed/frequency of each generator cannot be changed instantly according to the value requested from the frequency droop.

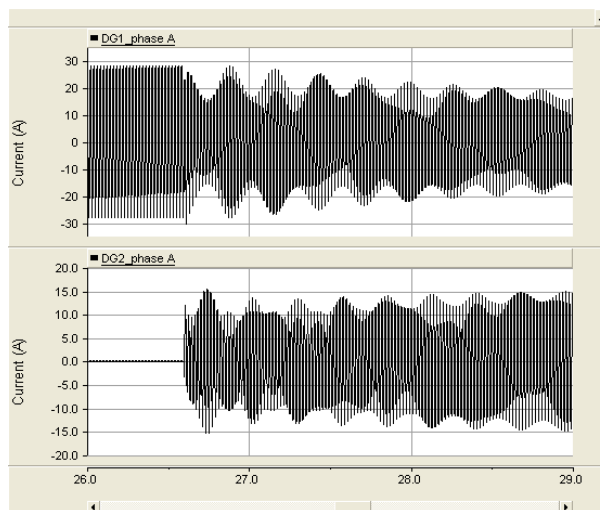


Fig. 7. The variation of DG output currents in phase-A.

The absence of a single strong source (such as utility grid) in an autonomous microgrid, these frequency oscillations manifest more vigorously. In the microgrid configuration of Fig. 4, the two diesel generators are separated by a small line segment, which does not provide sufficient damping. However, it is desirable to damp out these transient oscillations as quickly as possible from the view point of stability and power quality issues. Therefore, a research method is proposed to achieve a smooth droop transfer characteristic for the incoming diesel generator (i.e. for DG2). This is obtained by slowly changing the frequency setting of incoming generator from the PC frequency to the droop frequency. The characteristic for smooth droop transfer is implemented by modifying (1) as

$$f_d = f^* + (f^* - f_{pc}) \times \sqrt{\left(1 - \frac{t^2}{T_p^2}\right)} \times \left[u_s(t) - u_s(t - T_p) \right] \quad (3)$$

where f_d is the droop frequency of the incoming DG, f_{pc} is the measured frequency at PC and T_p is the time constant chosen to reach the droop frequency from the PC frequency. The time t is measured after the DG circuit breaker is closed. $u_s(t)$ is the unit time step function. The term inside the square brackets will be zero after the time T_p elapses, forcing the last term of (3) to be zero. Therefore the frequency of the incoming DG will be equal to the droop frequency calculated from (1). The value of T_p can be selected according to the diesel generator dynamics. As per (3), an ellipsoidal shape is selected to reach the droop frequency from the PC frequency. This shape is selected because the rate of change of frequency increases towards the droop line and becomes higher with the elapsed time. However, the frequency will not go out of bound as the last term of (3) becomes zero after the defined time

period T_p .

The simulation study performed before is repeated while applying the proposed modification in the droop control. Fig. 8 shows the response of real and reactive power output of DG1 and DG2. It can be seen that DG2 increases its output power gradually without the power fluctuations. The variation of DG frequency during and after the synchronization is shown in Fig. 9. It shows the DG2 frequency increases gradually until it reaches the droop frequency. These figures clearly indicate an improved dynamic performance, while the power sharing quality remains unchanged.

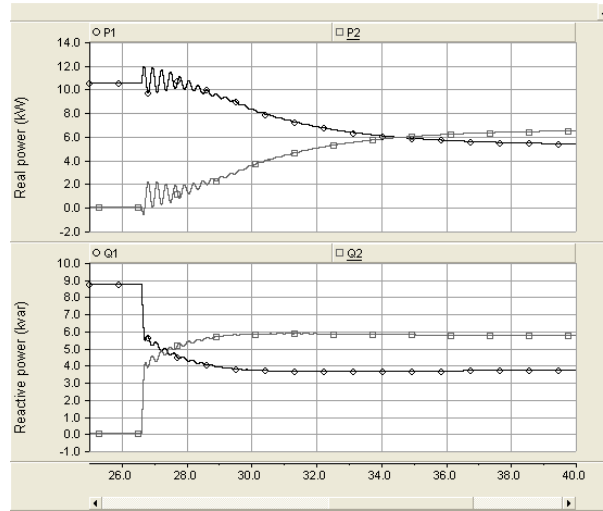


Fig. 8. Real and reactive power sharing with the modified droop.

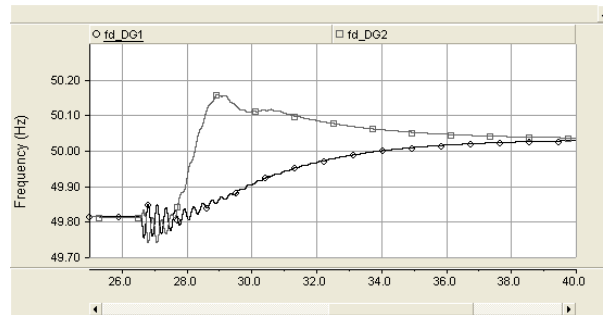


Fig. 9. The variation of DG droop frequencies with the modified droop.

3.2. Microgrid Operation with Non-Inertial DGs

For this case also we consider the same microgrid structure shown in Fig. 4. However, both DG1 and DG2 are now non-inertial sources which are connected through converters. Initially, DG1 supplies *load1* operating in frequency and voltage droop according to (1) and (2) respectively. DG2 is connected at 5.262 s once synchronizing conditions are satisfied. Subsequently, *load2* is connected to the microgrid at 7.0 s.

The real and reactive load power sharing of DGs are shown in Fig. 10. DG2 starts to inject real power soon after its connection to the microgrid. It further increases the output power once *load2* is connected. However, it can be seen that the system attains steady state within 0.2 s after either the DG synchronization or the load change. Also, the DGs share the real power more precisely according to their ratings (i.e. 1.25).

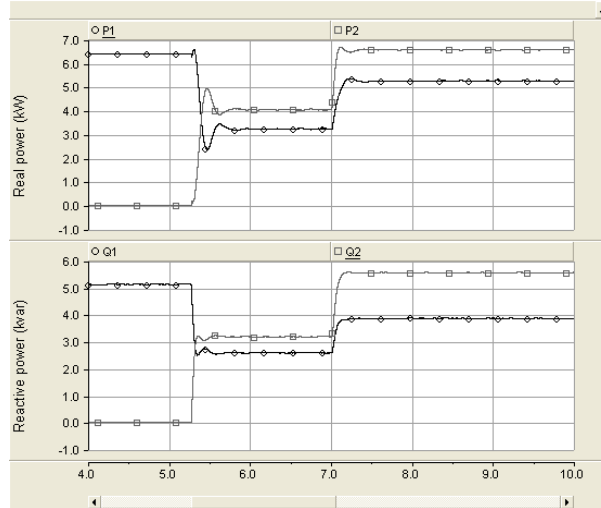


Fig. 10. The real and reactive power sharing with non-inertial DGs.

The variation of DG frequencies is shown in Fig. 11. After DG2 synchronization, DG2 frequency changes to no load frequency as calculated from the droop and then it reaches to steady state system frequency within one second. However, no frequency and real power fluctuations can be observed unlike the case of two diesel generators. The interaction between these two non-inertial DGs during synchronization and load change is smooth. Due to the fast response time of the converters, the steady state is attained very quickly.

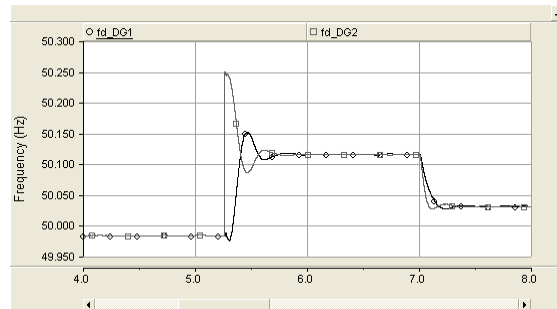


Fig. 11. The variation of droop frequencies of non-inertial DGs.

It can thus be concluded that if the microgrid only contains converter interfaced DGs, conventional frequency and voltage droop given in (1) and (2) can be used to share the real and reactive power without any appreciable transient oscillations.

3.3. Microgrid Operation with Inertial and Non-Inertial DGs

To study the interaction between an inertial and a non-inertial DG, the same microgrid structure, as shown in Fig. 4, is considered. It is assumed that DG1 is inertial based on diesel generator, while DG2 is non-inertial. In the simulation, *load2* is assumed to be equal to *load1*. Furthermore, it is assumed that DG1 is connected to the microgrid supplying *load1* operating in frequency and voltage droop control. DG2 is synchronized to the microgrid at 3.5 s. Subsequently, *load2* is connected to the microgrid at 6 s.

The real and reactive load power sharing amongst DG1 and DG2 is shown in Fig. 12. DG2 starts to inject real power after its connection. However, since the inertial DG1 responds

slowly, the non-inertial DG2 cannot increase the real power output quickly. Thus, the system takes 2-3 seconds to reach the steady state. The variation of DG frequencies is shown in Fig. 13. These results show that there are frequency and real power fluctuations during DG connection or load connection into the system. However, the magnitude of these fluctuations is low compared to the case where both inertial DGs are present. In this case of mixed DG sources, the inertial generator cannot change its output frequency/power instantly unlike the converter interfaced DGs. Therefore, the slower response of diesel generator can initiate frequency and real power fluctuations in the autonomous microgrid.

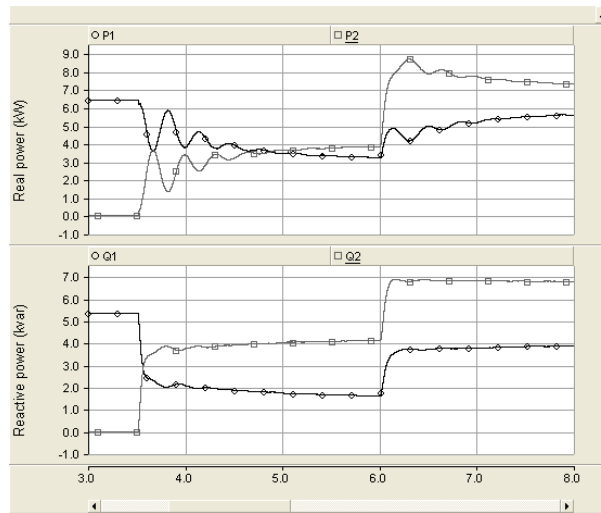


Fig. 12. Real and reactive power sharing with inertial and non-inertial DGs.

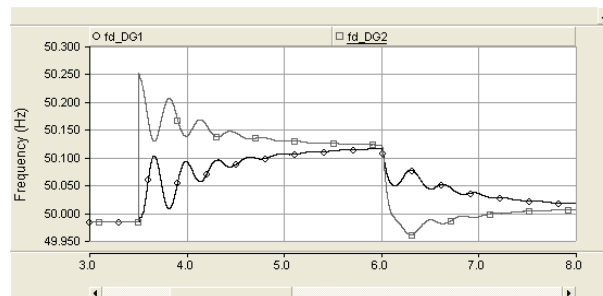


Fig. 13. The variation of DG droop frequency settings.

3.4. Angle Droop Control of Non-Inertial DGs

To minimize the transient oscillations in the presence of both inertial and non-inertial sources, a method is proposed, which takes into cognizance that a converter can change its output voltage angle instantaneously. Therefore, instead of droop frequency, a corresponding angle is set for the converter output voltage. This angle calculation corresponding to the droop frequency is explained in Appendix-B. As explained in this appendix, the angle for the converter output voltage can be calculated using

$$\phi = 2\pi \left[\frac{f^* - f_r}{f^*} \right] \quad (4)$$

where f_r is the rated frequency and f^* is the droop frequency. A phase lock loop (PLL) is used at PC to set the frequency for each DG converter voltage. Therefore, an angle (ϕ) corresponding to the frequency deviation (i.e., the amount of real power required to inject into the system) given by (4) is calculated and used in the converter reference generation. For example, if output feedback voltage control is used to control three phase converters [18], the reference voltages for three phases are generated using voltage magnitude obtained from voltage droop and calculated angle in (4). In this case, the reference of phase-A can be generated as

$$V_a = V_m \sin(2\pi f_{pc} t + \phi) \quad (5)$$

where V_m is the voltage magnitude calculated from the voltage droop in (2), f_{pc} is the measured frequency at PC using the PLL and ϕ is the angle calculated from (4). It is to be noted that the proposed method is only applicable if there is at least one inertial DG already connected to the microgrid. Since the microgrid frequency is mainly controlled by the inertial sources, the reference frequency of the non-inertial DG is basically controlled by them. Therefore, to avoid any transient oscillation, the PC frequency is used for reference voltage calculations.

For the case discussed in the previous sub-section, the real and reactive power sharing amongst the DGs is shown Fig. 14 after setting the DG2 angle according to (5). It is evident that there are no frequency and power oscillations during the synchronization and load change. However, it can be noticed that the accuracy of power sharing between the inertial DG and non-inertial DG is not as precise as that obtained from the conventional frequency droop.

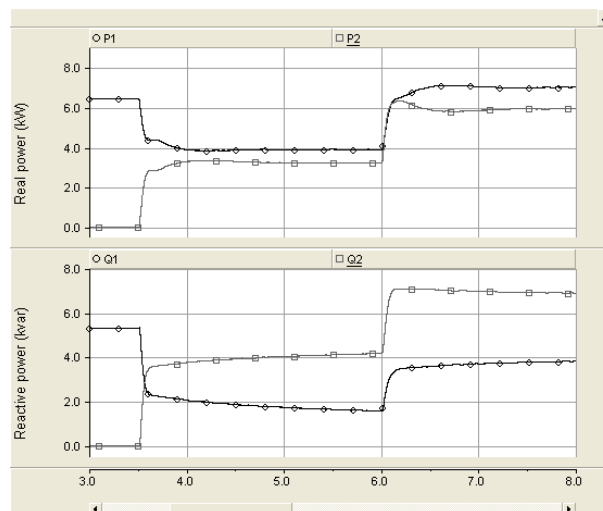


Fig. 14. Power sharing with angle based droop control.

4. Integral to Droop Line Control

To improve the real power sharing amongst these DGs further, a modified droop control characteristic is proposed for a microgrid containing both inertial and non-inertial DGs. This ensures that the change of load is proportionally picked up by all the DGs. The proposed droop control is called as the *integral to droop line* and is only implemented on the converter interfaced DGs in the microgrid. It has been shown in [19] that a high gain droop control is

preferable for accurate power sharing, but it can cause the system to be unstable, especially during transients. In the proposed droop control, the steady state and transient gains are set independently using an integral controller. Thus, system can respond with a medium gain during a transient event but reach a steady state point corresponding to a high gain. Once an appropriate time constant is selected for the integrator, converter interfaced DGs can respond in a similar manner as inertial DGs. This results in a smooth transition to steady state. To implement the proposed droop, the frequency droop is modified by introducing an integration process to reach the steady state frequency droop point in the system. The error between calculated droop frequency in (1) and frequency at the PC is passed through an integrator to force the operating frequency of DG to reach the steady state droop point within a defined time period. The proposed method not only has the ability to minimize transient instability but also ensures proper power sharing amongst DGs. The integral to droop line control is given by

$$f_d = f^* + \int (f^* - f_{pc}) dt \quad (6)$$

where f_d is the modified droop frequency setting for the DG, f^* is droop given in (1) and f_{pc} is the measured frequency at PC. The angle (ϕ) corresponding to modified droop frequency f_d in (6) is calculated using (4). The time constant of the integrator is selected according to the inertial DG dynamics (i.e., time constant of governor). The power sharing of DGs after deploying the proposed frequency droop in (6) and angle setting in (5) is shown in Fig. 15. According to this, the accuracy of power sharing has improved and the transient oscillations are avoided.

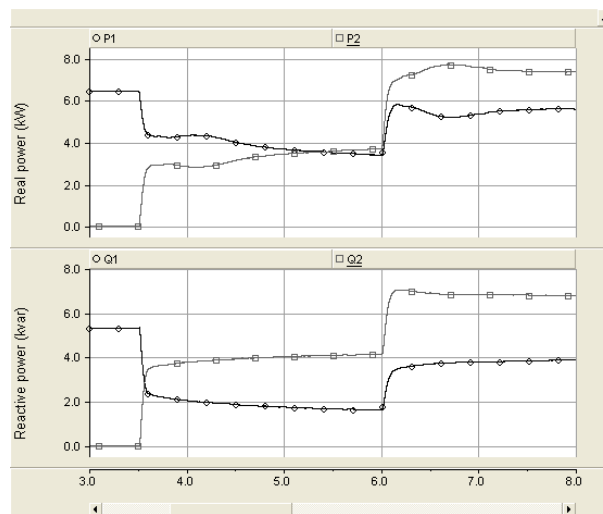


Fig. 15. Real and reactive power sharing with integral to droop line.

Key findings

In the presence of both inertial and non-inertial sources in a microgrid, conventional frequency droop can initiate frequency and real power oscillations during the synchronization and load changes. However these oscillations can be avoided if angle corresponding to the droop frequency is set in the converter voltage reference generation. It is shown that the proposed method of integral to system droop line has the ability to improve the dynamic power sharing amongst these inertial and non-inertial sources avoiding transient oscillations.

4.1. Further Investigation of Integral to Droop Line

To further illustrate the efficacy of proposed integral to droop line for a hybrid microgrid, the system shown in Fig. 16 is considered. In this system, a diesel generator is connected at BUS-1 while DG2 and DG3 which are interfaced through converters and are connected at buses 3 and 5 respectively. Three impedance type loads, *load1*, *load2* and *load3* are connected at buses 2, 4 and 6 respectively as shown in the figure. The converter interfaced DGs are operated in frequency droop control as according to (2), (5) and (6). Therefore, these DGs have the ability to control real and reactive power injection to the microgrid based on the angle and voltage reference settings. The parameters of the study system are given in Table 2.

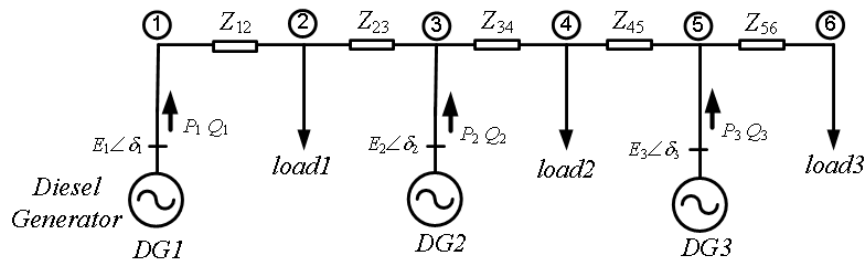


Fig. 16. Diesel generator with two converter interfaced DGs.

TABLE 2: PARAMETERS OF THE SYSTEM OF FIG. 16.

System data	Value
System frequency	50 Hz
System voltage	0.415 kV rms (L-L)
DG1 (diesel) power rating	(12 + j 8) kVA
DG2 power rating	(15 + j 10) kVA
DG3 power rating	(10 + j 6.7) kVA
Feeder impedance ($Z_{12}=Z_{23}=Z_{34}=Z_{45}$)	(0.025 + j 1.2566) Ω
Load impedance ($Ld1=Ld2=Ld3$)	(15 + j 11.781) Ω
Frequency droop coefficient (Hz/kW)	m1=0.0417, m2=0.033, m3=0.05
Voltage droop coefficient (V/kVAR)	n1=1.5, n2= 1.2, n3=1.791

The diesel generator supplies *load1* and *load2* while operating in frequency and voltage droop control in (1) and (2) respectively. Then DG2 and DG3 are connected to the microgrid at 3.5 s and 6.5 s respectively. Subsequently, *load3* is connected at 11.0 s. The real and reactive power sharing of DGs are shown in Fig. 17. As can be seen from the figure, DG1, DG2 and DG3 supply 6.23 kW, 7.83 kW and 5.26 kW respectively in the steady state in accordance to their droop gains. The results show that no power oscillation during DG connections and load changes due to the employment of integral to droop line in converter interfaced DGs.

The variation of microgrid frequency during the DG and load connections is shown in Fig. 18. It can be seen that system frequency increases with the DG connections and it reduces once *load3* is connected at 11 s. However, no appreciable oscillations in frequency can be observed. Fig. 19 shows the PC voltages of each DG. Each DG maintains its PC voltage according to the droop by injecting the required amount of reactive power into the

microgrid. It results in reactive power sharing amongst DGs maintaining the system voltage within the standard limits.

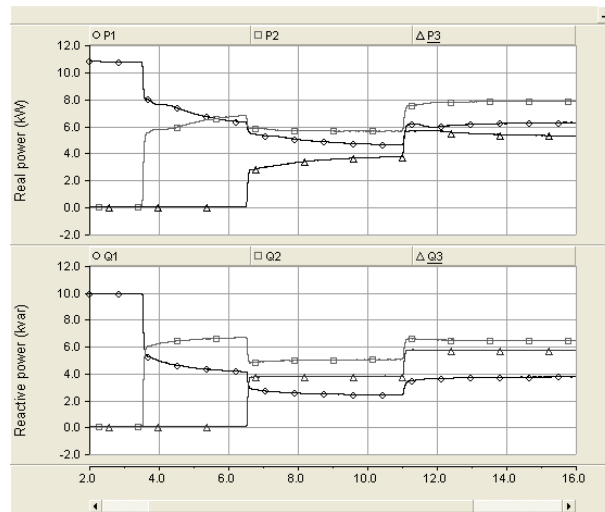


Fig. 17. Power sharing with diesel generator and two converter interfaced DGs.

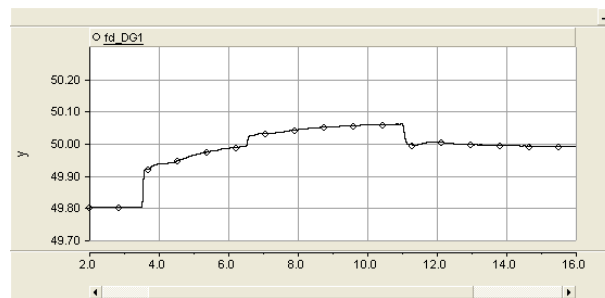


Fig. 18. The variation of system frequency.

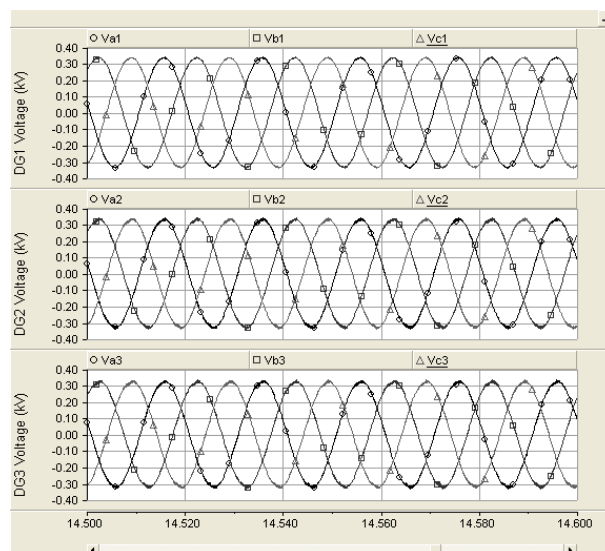


Fig. 19. Voltages at point of connection of DGs.

5. Microgrid Operation with Dispatchable and Non-Dispatchable DGs

A diesel generator is considered under dispatchable DG while a doubly fed induction generator (DFIG) is considered as a non-dispatchable DG to analyze the interaction in an autonomous microgrid. More details of DFIG model used for simulation are given in Appendix-C. In the developed model, the DFIG is operating in maximum power point (MPP) tracking injecting the maximum power available from the wind turbine. However, the DFIG is also capable of injecting reactive power into the microgrid if necessary. The deficit in the load power requirement is supplied by the diesel generator. The diesel generator can be controlled either in droop control or fixed frequency control mode. In this circumstance, fixed frequency control is selected since no other dispatchable DG is present to control the system frequency and share the load power. The output power of the DFIG will change with the time, while the diesel generator supplies the rest of load power requirement controlling the system frequency and voltage.

An autonomous microgrid containing a diesel generator and a DFIG as shown in Fig. 20 is considered for simulation studies. The selected feeder impedances and load impedances are the same as given in Table 2. Three constant impedance type loads are connected to the Bus-2. Initially, it is assumed that *load1* and *load2* are connected to the microgrid and supplied by the diesel generator and the DFIG. DFIG is set to inject zero reactive power into the system. In this case, wind speed for the wind turbine is selected as 12 m/s. Further, it is assumed that wind speed has gradually changed from 12 m/s to 13 m/s between 14 s and 16 s. Therefore the DFIG increases its output power operating in MPPT from 7.54 kW to 9.76 kW. This results in decreasing the power supplied by the diesel generator from 6.41 kW to 4.29 kW. The real and reactive power sharing amongst the diesel generator and the DFIG are shown in Figs. 21 and 22 respectively. It can be seen that DFIG increases its real power output with the change of wind speed while injecting zero reactive power into the microgrid.

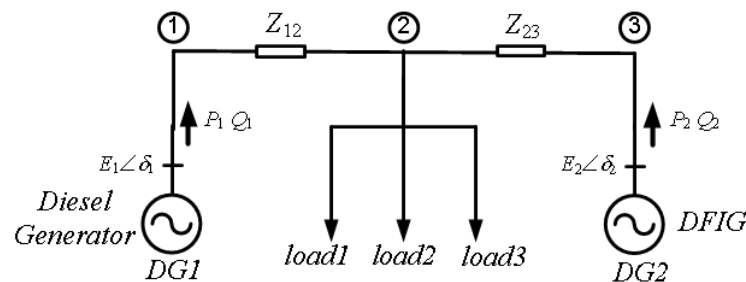


Fig. 20. Microgrid with a diesel generator and a DFIG.

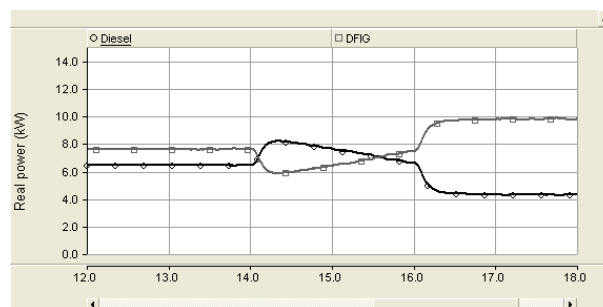


Fig. 21. Real power sharing amongst diesel generator and DFIG.

The output current of DFIG is shown in Fig. 23 and the voltage at PC of the DFIG is shown in Fig. 24. These results justify the smooth operation of DFIG in the isolated microgrid with the diesel generator.

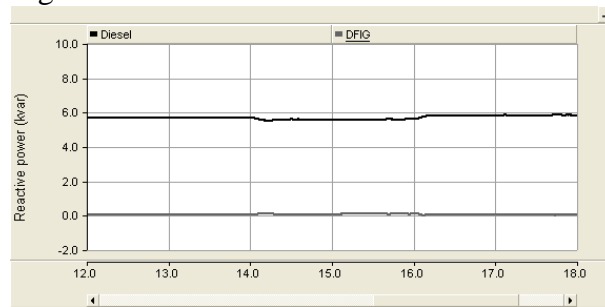


Fig. 22. Reactive power sharing amongst diesel generator and DFIG.

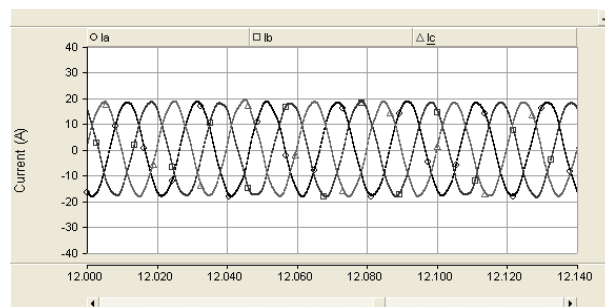


Fig. 23. Output currents of DFIG.

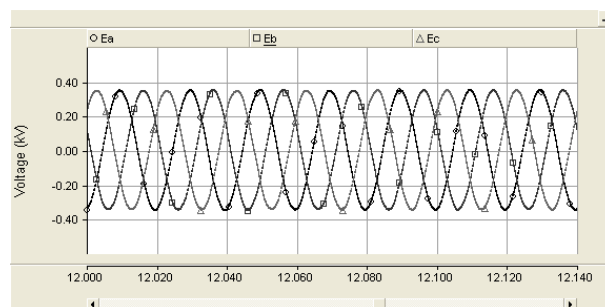


Fig. 24. PC voltage of DFIG (voltage at Bus-3).

Next, the effect of load change on the power sharing is investigated. In this case, it is assumed that the diesel generator and the DFIG supply *load1* and *load2* at the beginning and *load3* is connected at 6 s. Also, the reactive power output of DFIG is set to 2 kvar to illustrate the ability of reactive power injection of DFIG into the microgrid. The real and reactive power sharing amongst these two DGs are shown in Figs. 25 and 26 respectively. It can be seen that, DFIG injects the same amount of real and reactive power (i.e., 7.28 kW and 2 kvar) to the microgrid before and after the load change since it operates in MPPT. Therefore, the diesel generator has to increase its real and reactive power output to supply the power to the incoming load. The torque produced by the diesel engine during the load connection is shown in Fig. 27. It can be seen that torque of the diesel engine has increased to supply the incoming load. However, the frequency of the microgrid is maintained at nominal 50 Hz by the diesel generator.

The simulation results show that DFIG is capable of operating in MPPT while injecting reactive power into the microgrid if required. The diesel generator is required to supply the balance of the load power requirement in the microgrid. Here no droop control is required for the diesel generator since there is no other dispatchable DG available to share the real power requirement with the diesel generator.

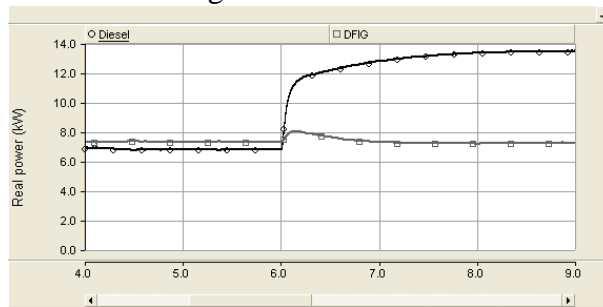


Fig. 25. Real power sharing during load change with diesel generator and DFIG.

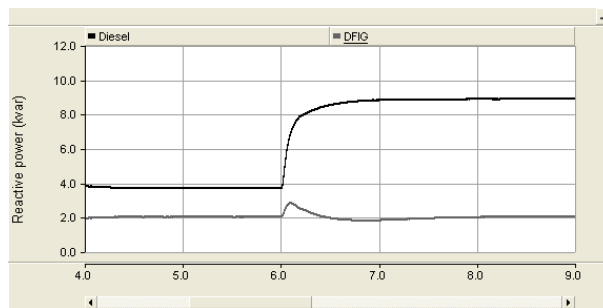


Fig. 26. Reactive power sharing during load change with diesel generator and DFIG.

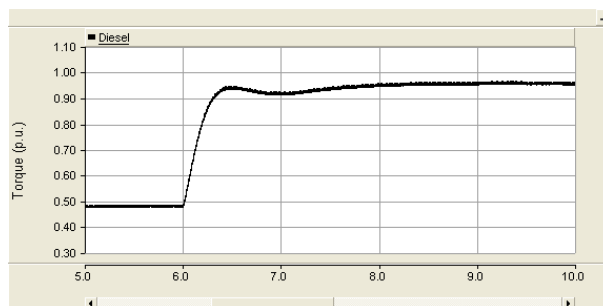


Fig. 27. Change of output torque in diesel generator.

6. Microgrid Operation with Inertial, Non-Inertial, Dispatchable and Non-Dispatchable DGs

This study is carried out to investigate the control and power sharing of an autonomous microgrid in the presence of different DG types. The DGs considered in the study can be categorized either as inertial or non-inertial DGs or dispatchable or non-dispatchable DGs. The study microgrid is shown in Fig. 28. DG1 is a diesel generator, DG2 is a DFIG and DG3 is connected to the microgrid through a converter. Three loads are connected to the microgrid as shown in the figure. The parameters of the study system are given in Table 3.

The DFIG (the non-dispatchable DG) is operated in MPPT. The diesel generator and the converter interfaced DG are controlled in frequency and voltage droop to share the rest of the load power requirement according to a predefined ratio. Diesel generator is employed with frequency droop in (1) while the converter interfaced DG is controlled using the integral to droop line given in (5) and (6).

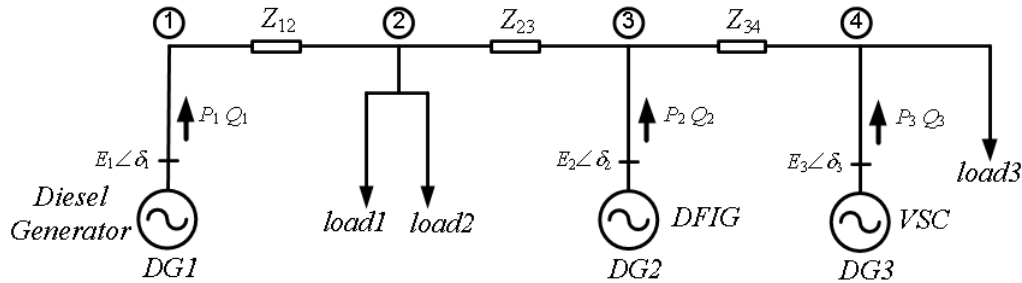


Fig. 28. Microgrid with diesel generator, DFIG and converter interfaced DG.

TABLE 3: PARAMETERS OF THE SYSTEM OF FIG. 28.

System data	Value
System frequency	50 Hz
System voltage	0.415 kV rms (L-L)
DG1 (diesel) power rating	(12 + j 8) kVA
DG2 (DFIG) power rating	(10 + j 6) kVA
DG3 (VSC) power rating	(10 + j 6.7) kVA
Feeder impedance ($Z_{12}=Z_{23}=Z_{34}$)	(0.0833+ j 0.8357) Ω
Load impedance	
load1	(15+ j 11.781) Ω
load2	(15+ j 11.781) Ω
load3	(15+ j 11.781) Ω
Frequency droop coefficient (Hz/kW)	
DG1	m1=0.0417
DG3	m3=0.05
Voltage droop coefficient (V/kVAR)	
DG1	n1=1.5
DG3	n2=1.8

At the beginning, it is assumed the diesel generator and the DFIG supply the *load1* and *load2*. DG3 is then connected to microgrid at 6 s. Next *load3* is connected to microgrid at 10 s. No change in wind speed has been assumed here. The reactive power output of the DFIG is set to 2 kvar. The real power sharing amongst DGs are shown in Fig. 29 during the DG3 and *load3* connections. Before DG3 is connected to microgrid, DG1 and DG2 inject 6.83 kW and 7.3 kW to the system. However, after DG3 is connected to the microgrid, DG2 power output remains as same, while DG1 decreases its output power and DG3 increases its power output. In steady state, power output of DG1 and DG3 become 3.92 kW and 3.13 kW as expected from the droop coefficients. Furthermore, after *load3* is connected, DG1 and DG3 supply the new load power demand operating in the droop control. The reactive power outputs of the DGs are shown in Fig. 30.

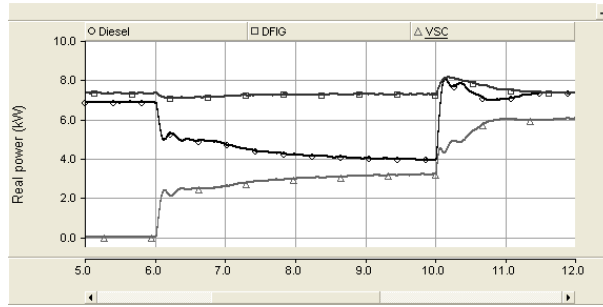


Fig. 29. Real power sharing with diesel generator, DFIG and converter interfaced DG.

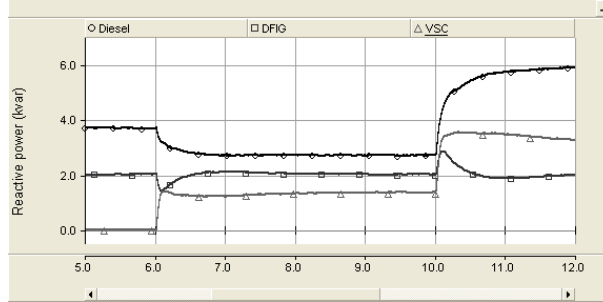


Fig. 30. Reactive power sharing with diesel generator, DFIG and converter interfaced DG.

The variation of system frequency during the DG3 and load3 connections is shown in Fig. 31. In this situation, the system frequency is mainly controlled by the DG1 operating in droop, since DG3 used this frequency as a reference to supply the required amount of real power into the microgrid. The variation in the converter output voltage angle related to the droop frequency is shown in Fig. 32. It can be seen that, angle is integrated toward steady state droop line to achieve a precise real power sharing.

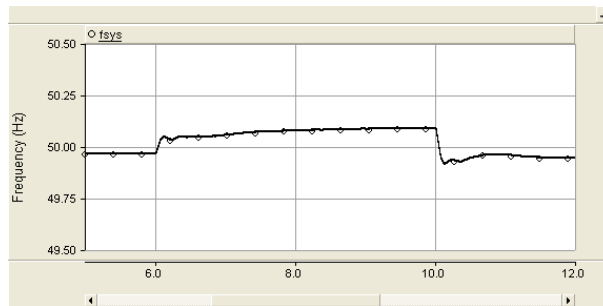


Fig. 31. The variation of system frequency.

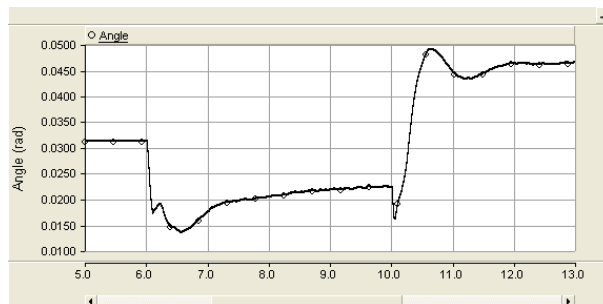


Fig. 32. The variation of VSC droop angle setting.

In the studies presented above, only DFIG type non-dispatchable DG has been considered. We have also discussed PV model and its characteristics in Appendix D. However, this model has not been included in the simulation studies. A PV is also a non-dispatchable source that works in MPPT, similar to a DFIG. The only difference is that it may not be able to supply the required amount of reactive power due to its converter size limitation.

7. Incorporation of Battery Storage into a Microgrid

In this section, power management and control strategies required to incorporate non-schedulable (renewable energy based) DGs and battery storage into a microgrid are discussed. The microgrid can include diesel generator(s), battery storage (BS), wind and solar PVs. The control of microgrid should enable the plug and play capability of DG sources, thus maximizing the benefits of renewable based energy sources. Decentralized control amongst DG sources is proposed as a simple and cost effective solution. Each DG has its own local control for connection and disconnection from the microgrid, and for controlling the real and reactive power output.

The BS is connected to the microgrid through a converter ensuring bidirectional power flow between microgrid and battery. Therefore, the BS can act as either a load or a source to absorb or inject real power into the microgrid. Also, the BS can assist in controlling the microgrid frequency. Moreover, the converter associated with BS has the ability to regulate the voltage at PC by injecting reactive power into the microgrid. The converter rating determines the maximum reactive power injection capacity into the system. The BS is employed with an intelligent control system (ICS) (or battery management system (BMS)) to manage the power effectively. The ICS in BS is continuously monitoring the state of charge (SOC) of the battery. If the battery is not fully charged and there is surplus power in the microgrid, the surplus power is used to charge the batteries. The battery storage can be controlled as “operating reserve” to supply or absorb any transient power during changes in generation or loads within the energy limits. For example, when the load changes in the microgrid, the BS can react very quickly to match the load power change. The ICS is responsible for managing the operating reserve in the battery and controlling the battery charging and discharging.

The DGs connected through wind and PVs are controlled using maximum power point tracking (MPPT) to enhance the benefits of renewable energy sources. Therefore, any deficit in load power is supplied by other dispatchable sources (i.e., diesel, BS) operating in frequency and voltage droop control. Voltage control of each dispatchable DG and voltage droop amongst DGs ensures the voltage regulation, stability and proper reactive power sharing, avoiding reactive power circulation in the microgrid. The proposed frequency droop lines for BS and diesel generator are defined to ensure the battery is charged when there is excess power available in the microgrid.

The droop lines for the diesel generator and BS are shown by *DE* and *AFG* respectively in Fig. 33. The line segment *AF* represents the droop for battery charging while the droop for battery discharging is represented by line *FG*. According to the droop lines shown in Fig. 33, BS starts to supply the load power once the diesel generator reaches its maximum power output at rated frequency. However, it is to be noted that slope of the droop line is controlled by the ICS and it can be changed towards points *H* or *K*. The reason for

8. Conclusions

Dynamic response of inertial (rotating direct connected) and non-inertial (converter interfaced) DGs in a microgrid is different. The inertial based DGs show a slower response while non-inertial DGs can respond very quickly. This mismatch of response rate in different DGs creates transient oscillations in an autonomous microgrid where no strong is present to control the system frequency and voltage. Moreover, power management strategies are required in the presence of both dispatchable and non-dispatchable DGs in the microgrid.

In this report, better control strategies are proposed for a hybrid microgrid operating in autonomous mode to improve the transient behavior and dynamic load power sharing. The proposed modified droop control for an inertial DG minimizes the frequency and real power oscillations during DG synchronization. Moreover, an angle based droop control strategy called integral to droop line is proposed for converter interfaced DGs to enhance a better dynamic power sharing while minimizing transient oscillations in the microgrid. Also, power management strategies are presented to incorporate both dispatchable and non-dispatchable DGs in the microgrid. It has been shown that proposed control and power management strategies have the ability to improve the microgrid performance.

9. References

- [1] S. J. Ahn, J. W. Park, I. Y. Chung, S. I. Moon, S. H. Kang, and S. R. Nam, "Power-Sharing Method of Multiple Distributed Generators Considering Control Modes and Configurations of a Microgrid," *IEEE Trans. Power Delivery*, vol. 25, pp. 2007-2016, 2010.
- [2] F. Katiraei, R. Iravani, N. Hatziargyriou, and A. Dimeas, "Microgrids management," *IEEE Power & Energy Magazine*, vol. 6, pp. 54-65, 2008.
- [3] J. Svensson, "Synchronisation methods for grid-connected voltage source converters," *IEE Generation, Transmission and Distribution*, vol. 148, pp. 229 - 235, 2001.
- [4] F. Katiraei and M. R. Iravani, "Power management strategies for a microgrid with multiple distributed generation units," *IEEE Trans. Power Systems*, vol. 21, pp. 1821-1831, Nov. 2006.
- [5] M. Shahabi, M. R. Haghifam, M. Mohamadian, and S. A. Nabavi-Niaki, "Dynamic Behavior Improvement in a Microgrid with Multiple DG Units Using a Power Sharing Approach," in *Proc. IEEE Bucharest Power Tech Conference*, 2009.
- [6] T. C. Green and M. Prodanović, "Control of Inverter-based Micro-grids," *Electric Power Systems Research*, vol. 77, pp. 1204-1213, July 2007.
- [7] Z. H. Jiang and X. W. Yu, "Active Power - Voltage Control Scheme for Islanding Operation of Inverter-Interfaced Microgrids," in *Proc. IEEE Power & Energy Society General Meeting*, pp. 1738-1744, 2009.
- [8] J. A. P. Lopes, C. L. Moreira and A. G. Madureira, "Defining Control Strategies for MicroGrids Islanded Operation," *IEEE Trans. Power Systems*, vol. 21, pp. 916-924, 2006.
- [9] H. H. Zeineldin, E. F. El-Saadany and M. M. A. Salama, "Distributed Generation Micro-Grid Operation: Control and Protection," in *Proc. IEEE Power Systems Conf.: Advanced Metering, Protection, Control, Communication, and Distributed Resources*, 2006.
- [10] K. D. Brabandere, B. Bolsens, J. V. d. Keybus, A. Woyte, J. Driesen, and R. Belmans, "A Voltage and Frequency Droop Control Method for Parallel Inverters," *IEEE Trans. Power Electronics*, vol. 22, pp. 1107 - 1115, 2007.
- [11] L. Zhang, L. Harnefors and H.-P. Nee, "Power-Synchronization Control of Grid-Connected Voltage-Source Converters," *IEEE Trans. on Power Systems*, vol. 25, pp. 809 - 820, 2010.

- [12] J. A. P. Lopes, C. L. Moreira and A. G. Madureira, "Defining control strategies for microgrids islanded operation," *IEEE Trans. Power Systems*, vol. 21, pp. 916-924, May 2006.
- [13] M. C. Chandorkar, D. M. Divan and R. Adapa, "Control of parallel connected inverters in standalone AC supply systems," *IEEE Trans. Industry Applications*, vol. 29, pp. 136 - 143 1993.
- [14] S. Krishnamurthy, T. M. Jahns and R. H. Lasseter, "The Operation of Diesel Gensets in a CERTS Microgrid," in *Proc. IEEE Power & Energy Society General Meeting*, 2008.
- [15] R. Majumder, A. Ghosh, G. Ledwich, and F. Zare, "Control of parallel converters for load sharing with seamless transfer between grid connected and islanded modes," in *Proc. IEEE Power and Energy Society General Meeting*, 2008.
- [16] R. Majumder, A. Ghosh, G. Ledwich, and F. Zare, "Angle Droop Versus Frequency Droop in a Voltage Source Converter Based Autonomous Microgrid," in *Proc. IEEE Power & Energy Society General Meeting*, 2009.
- [17] R. Majumder, F. Shahnia, A. Ghosh, G. Ledwich, M. Wishart, and F. Zare, "Operation and Control of a Microgrid Containing Inertial and Non-Inertial Micro Sources," in *Proc. IEEE Region 10 Conference (Tencon)*, Singapore, 2009.
- [18] A. Ghosh, K. Jindal and A. Joshi, "Inverter control using output feedback for power compensating devices," *Proc. IEEE Asia-Pacific Region-10 Conference TENCON*, Bangalore, 2003, pp. 49-52.
- [19] R. Majumder, B. Chaudhuri, A. Ghosh, R. Majumder, G. Ledwich and F. Zare, "Improvement of stability and load sharing in an autonomous microgrid using supplementary droop control loop," *IEEE Trans. Power Systems*, Vol. 25, No. 2, pp. 796-808, 2010.

Appendix-A: Diesel Generator Modeling and Control

A diesel generator set consists of an internal combustion (IC) engine coupled to a synchronous generator. The schematic diagram of the generator set is shown in Fig. A.1. The IC engine is integrated with a governor for controlling the output speed of the engine shaft by adjusting the amount of fuel supplied to the engine. There is a dead time associated with the change of fuel supply to the change in output torque of the IC engine due to its inertia. The governor is controlled by using a PID controller. The synchronous generator is incorporated with an exciter and a voltage regulator. The voltage regulator controls the field supply of the generator to maintain the required terminal voltage. The mathematical model of a diesel generator set is not explained here and it can be found in [A1-A3]. The diesel generator model is developed with the appropriate controls in PSCAD for the microgrid simulation studies.

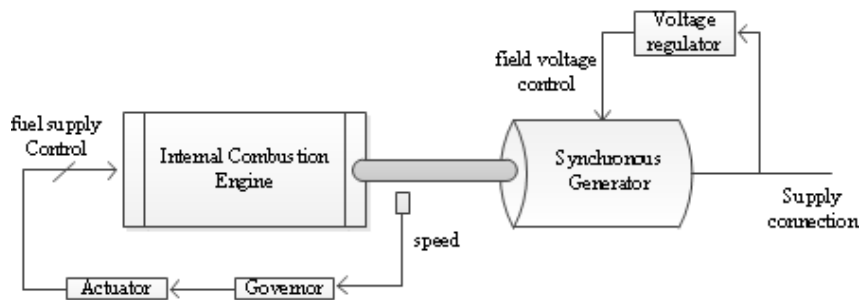


Fig. A.1. Schematic diagram of the diesel generator set.

The diesel generator set has the ability to operate in frequency and voltage droop control modes. In the droop control mode, the IC engine maintains the required output shaft speed to a value requested by the frequency droop while the terminal voltage is adjusted to the value requested by the voltage droop.

Simulation studies of the diesel generator set are performed to investigate the transient behavior of a standalone system. For this, we have considered a diesel generator that supplies two impedance loads, as shown in Fig. A.2. The parameters of the diesel generator are given in Table A.1. The response of the diesel generator under different circumstances is considered. First two scenarios show the response during load connection and load disconnection while last case shows the response when generator operates in frequency and voltage droop control.

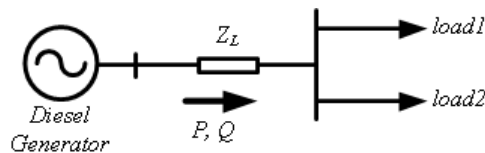


Fig. A.2. Diesel generator set connected to loads.

(i). *The response of the diesel generator during load connection*

In this study, it is assumed that the diesel generator initially supplies only the *load1*. Consequently, *load2* is connected at 8 s. The variation of system frequency is shown in Fig. A.3. As can be seen from the figure, the frequency of the system drops immediately after the

load connection. However, the system frequency attains to the steady state after around 1 s. This response is due to the governor dynamics in the diesel engine. This can be further seen from the change of output torque in the IC engine as shown in Fig. A.4. The engine increases its output torque due to the increase in load to maintain a constant output speed.

TABLE A.1: THE PARAMETERS OF THE DIESEL GENERATOR SET.

System data	Value
Rated voltage	415V
Rated power	12kW, 14.4kVA
Rated frequency	50Hz
Rated speed	1500 rpm
Reactance	Value (per unit)
X_d	2.26
X'_d	0.15
X''_d	0.060
X_q	0.13
X''_q	0.107
X_2	0.91
X_0	0.005
Time constants	Value (ms)
t'_d	25
t''	25
t'_{d0}	368
t_a	4

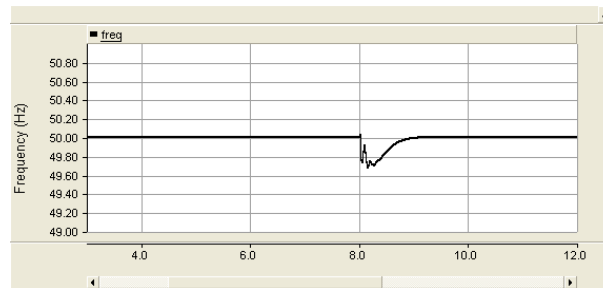


Fig. A.3. The variation of system frequency during a load connection.

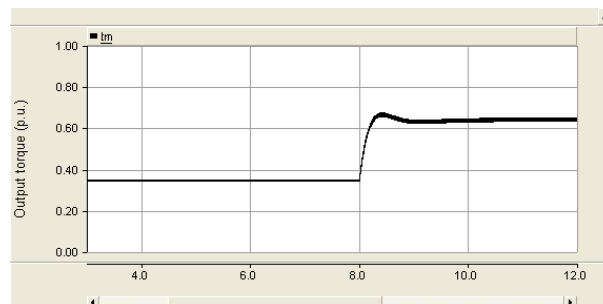


Fig. A. 4. The variation of output torque of the engine during a load connection.

The variation of RMS terminal voltage in phase-A is shown in Fig. A.5. This characteristic shows the behavior of the voltage regulator during the load change. The real and reactive power output of diesel generator is shown in Fig. A.6.

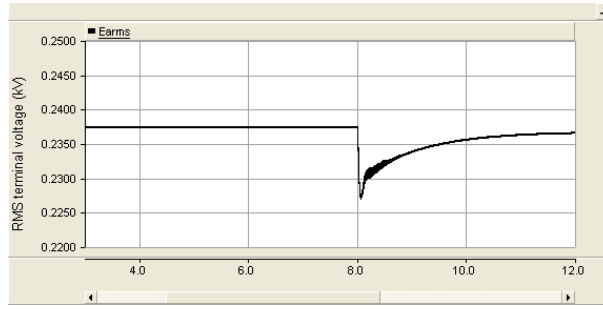


Fig. A. 5. The variation of RMS terminal voltage during a load connection.

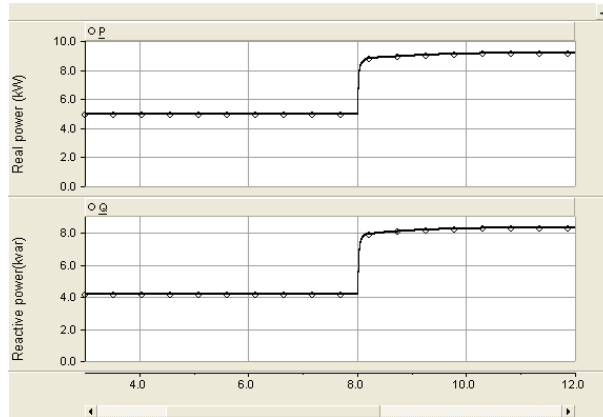


Fig. A. 6. The variation of real and reactive power during a load connection.

(ii). The response of the diesel generator during a load disconnection

It is assumed that the diesel generator initially supplies *load1* and *load2*. Subsequently, *load2* is disconnected at 8 s. The variation of system frequency and RMS voltage during the load disconnection is shown in Figs. A.7 and A.8 respectively. The frequency and voltage increase during the system transient. The real and reactive power supplied by the diesel generator is shown in Fig. A.9.

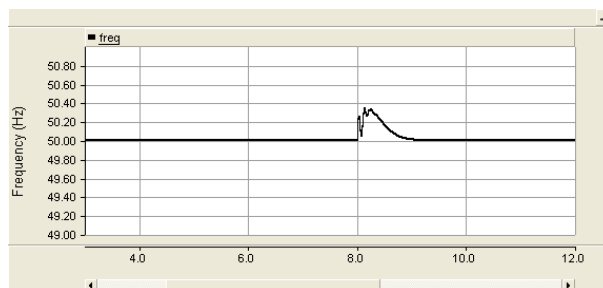


Fig. A.7. The variation of system frequency during a load disconnection.

(iii). The response of the diesel generator with the droop control

In this study, it is assumed that the diesel generator is connected to *load1* and *load2* operating in frequency and voltage droop control mode. Then *load2* is disconnected at 8 s. The variations in frequency and voltage are shown in Figs. A.10 and A.11 respectively. It can be seen that the system frequency and voltage have slightly increased due to the load

disconnection. Since droop has been activated, the system frequency and voltage will vary depending on the generator real and reactive power output. Moreover, the amount of frequency and voltage deviation from the nominal value will be dependent on the selected droop coefficients.

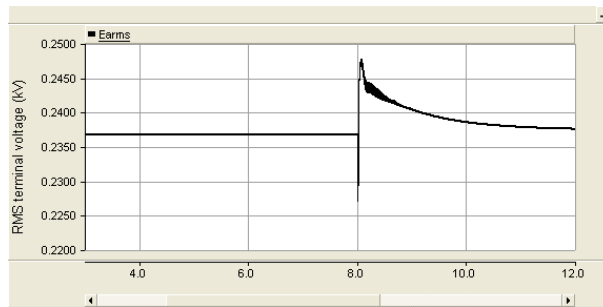


Fig. A. 8. The variation of generator terminal voltage during a load disconnection.

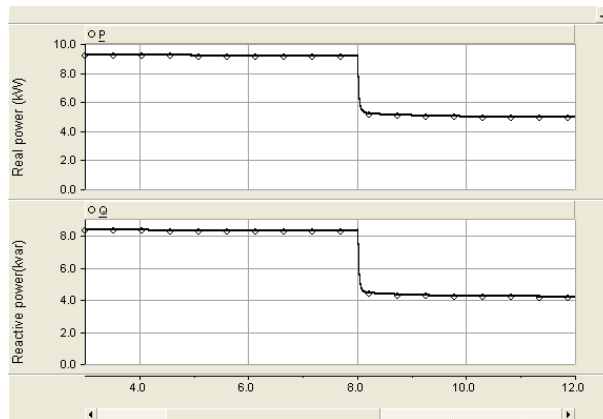


Fig. A.9. Real and reactive power change during a load disconnection.

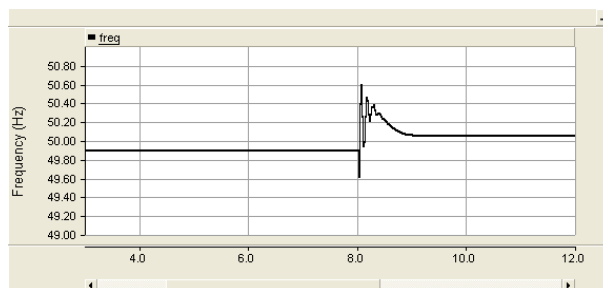


Fig. A.10. The variation of frequency in droop control.

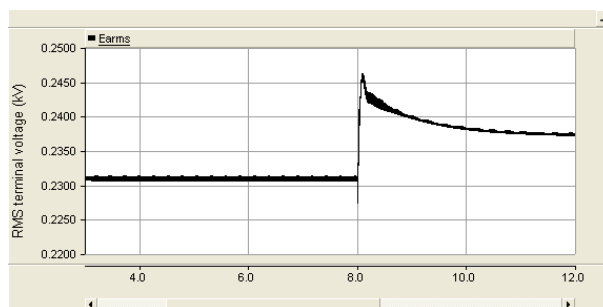


Fig. A. 11. The variation of terminal voltage in droop control.

The simulation results show that the diesel generator can be operated either in fixed speed mode (i.e., constant frequency) or droop control mode. However, during load changes in the system, the generator takes finite time period to attain to the steady state irrespective of the operating mode due to its inertial behavior.

References

- [A1] D. Yubing, G. Yulei, L. Qingmin and W. Hui, "Modelling and simulation of the microsources within a microgrid," *International Conference on Electrical Machines and Systems*, pp. 2667 - 2671, 2008.
- [A2] B. Kuang, Y. Wang and Y. L. Tan, "An H_∞ controller design for diesel engine systems," *International Conference on Power System Technology*, pp. 61 - 66, 2000.
- [A3] H. Yasin, A. A. EI-Zeftawy, M. N. Serag, and A. A. Gado, "Design of a controller for operating Diesel Generator to supply isolated loads," *Eleventh International Middle East Power Systems Conference*, pp. 487 – 491, 2006.

Appendix-B: DG Output Voltage Angle Calculation

Let the rated frequency of the system be denoted by f_r while the calculated droop frequency for a DG using frequency droop be denoted by f^* . The droop frequency, f^* represents the amount of frequency deviation from its rated value. The variation of angular frequency vectors related to f_r and f^* is shown in Fig. B.1. It can be seen that angular vector corresponding to f_r reaches 2π at time t_1 while angular vector related to f^* reaches 2π at time t_2 . In this figure, it is assumed that $f_r > f^*$.

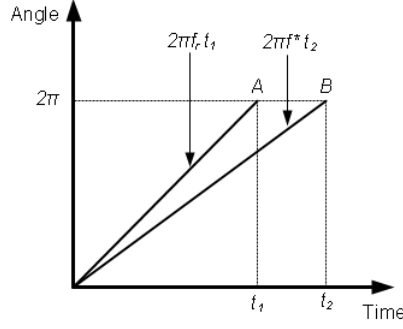


Fig. B.1. The variation of angular vectors.

From Fig. B.1, we can write

$$2\pi = 2\pi f_r t_1 = 2\pi f^* t_2 \quad (\text{B.1})$$

The angular vector related to the droop frequency can be expressed in terms of rated frequency and an angle difference ϕ such that the condition in (B.1) is satisfied. Then it can be written as

$$2\pi f^* t_2 = 2\pi f_r t_2 + \phi \quad (\text{B.2})$$

Using (B.1) and (B.2), the angle difference can be calculated as

$$\phi = 2\pi \left(\frac{f^* - f_r}{f^*} \right) \quad (\text{B.3})$$

Therefore the required angle corresponding to the droop frequency can be found using the rated frequency and calculated droop frequency. The reference voltage generation of each phase of the converter is then performed with the aid of calculated angle in (B.3).

Appendix-C: Doubly Fed Induction Generator (DFIG) Modeling and Control

Wind energy is one of the best technologies available today to supply the rapid load growth demand. Because power generation based on wind energy is considered to be economical and non-polluting. Thus there is a significant trend towards increasing the wind penetration throughout the worldwide. There are different types of wind power topologies available to extract power from the wind [C1].

- (i) Fixed speed induction generators
- (ii) Variable speed, pitch controlled synchronous generators
- (iii) Variable speed, pitch controlled doubly fed induction generators (DFIG)

Among these available topologies, doubly fed induction generator (DFIG) which utilizes two back-to-back converters is emerging as the preferred technology [C2]. Because the DFIG based wind turbines can operate under variable speed range. These DFIGs can be operated at any desired power factor controlling the converters [C1]. These variable speed DFIGs have advantages compared to the fixed speed generators. Lower cost of converters, acoustic noise reduction, capable of absorbing more power and simple pitch control are few of the advantages. A DFIG is also capable of operating in four quadrants of active and reactive powers [C3]. Thus, the ability of generating electricity at different power factors reduces the cost for reactive power compensators in a network [C4]. Also, these DFIGs can absorb gusts of wind reducing the mechanical stress and torque pulsations [C5].

The wind turbine converts the kinetic energy of wind into the mechanical power. The mechanical power output available at the turbine can be expressed by following equation [C2, C4].

$$P_w = \frac{1}{2} \rho \pi R^2 v^3 C_p(\theta, \gamma) \quad (\text{C.1})$$

where ρ is the air density, R is the radius of the turbine, v is the wind speed and C_p is the power coefficient. The power coefficient C_p is a function of pitch angle (θ) and the tip speed ratio (γ) which is defined as

$$\gamma = \frac{\omega_w R}{v} \quad (\text{C.2})$$

where ω_w is the turbine rotor speed. The relationship between power coefficient and tip speed ratio is shown in Fig. C.1.

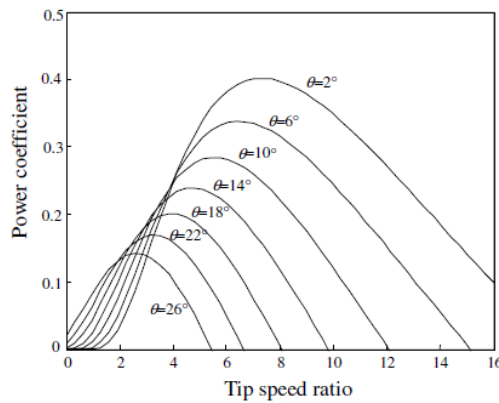


Fig. C.1. The variation of power coefficient with tip speed ratio (adapted from [C2]).

The output torque of the turbine can be given as

$$T_w = \frac{P_w}{\omega_w} \quad (C.3)$$

The wind speed may change over a large range. According to (C.1), the mechanical power increases when wind velocity increases. Therefore the input power to the generator should be controlled with the change of wind speed such that it will not exceed the rated power. The extracted wind power can be controlled by either varying the tip speed ratio or pitch angle [C1]. A typical characteristic of wind power control with the change of wind speed is shown in the Fig. C.2.

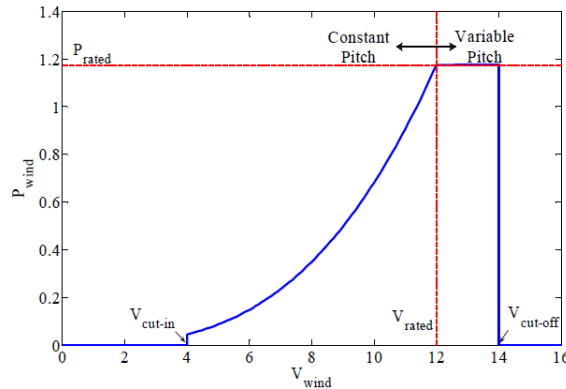


Fig. C.2. The characteristics of wind power with wind speed (adapted from [C1]).

In low and moderate wind speed, the maximum power coefficient is maintained by maximizing the tip speed ratio [C2]. However, in high wind speed, the output power is controlled at the rated power of the generator by decreasing the power coefficient. The control of power coefficient can be achieved either changing the pitch angle or generator rotational speed. The pitch angle can be controlled to change the extracted power from the wind while the applied rotor voltage (or current) and frequency can be controlled to change the rotor speed. The set point for the rotor speed is calculated based on the optimal tip speed ratio at a given wind speed [C6]. The pitch control is usually activated in high wind speed to decrease the power capturing from wind [C2, C5]. How the power coefficient can change with wind speed is shown in Fig. C.3.

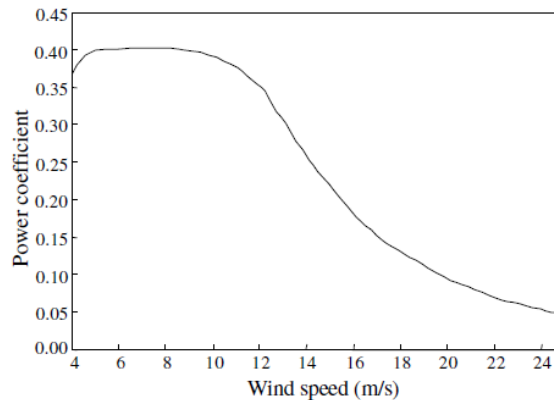


Fig. C.3. The variation of power coefficient for different wind speeds (adapted from [C2]).

The schematic diagram of a DFIG is shown in C.4. The stator of the DFIG is directly connected to the grid while rotor is connected to the grid via back-to-back converters. These two voltage source back-to-back converters in which one converter is connected to the rotor (rotor side converter-RSC) and the other is connected to the grid side (grid side converter-

GSC) can be used to control the direction and magnitude of the power flow [C7]. The rotor winding of the induction machine is fed by the RSC with a voltage at the slip frequency. The voltage magnitude and the phase angle are calculated according to the present turbine speed. These converters only supply the slip power requirement for the wound rotor induction generator [C8]. Therefore, converters can be designed with a lower power rating usually the range around 25-30 % of the generator rating [C3, C9-C11]. This results in the reduction of power loss and the cost associated with the converters and filters. Basically the RSC controls the real and reactive power output while the GSC controls the dc-link voltage and reactive power absorbed from the grid [C11]. The over voltage and overcurrent protection are incorporated in the machine and the converters by means of a crowbar circuit [C12].

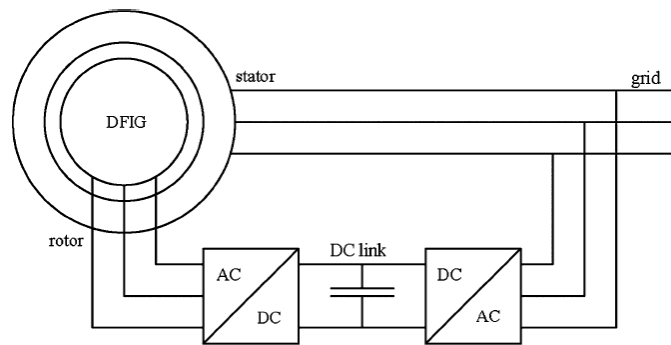


Fig. C.4. Schematic diagram of a DFIG.

The induction machines have three operating modes: motoring, generating and braking. The different operating modes and power flow directions of a slip ring induction machine are given in Table C.1. The DFIG can operate either sub-synchronous (slip > 0) or super-synchronous (slip < 0) mode depending on the present wind speed [C7]. The RSC should have the ability to operate under bidirectional power flow to cover wide range of sub-synchronous to super-synchronous speeds [C4]. In sub-synchronous mode, the speed of the rotor is less than the machine synchronous mode while the rotor speed is higher than the machine synchronous mode if it operates in super-synchronous mode. Traditional wound rotor induction generators never produce power at sub-synchronous mode [C7]. The RSC should be controlled properly to generate power under sub-synchronous mode. The power flow direction will change based on the operating mode. In sub-synchronous mode, the power flow into the rotor while it is in super-synchronous mode, power flows out of the rotor. The different operating modes of a DFIG can be represented as shown in Fig. C.5. The implementation of this four quadrant operation of a DFIG is possible with the control of RSC [C7].

TABLE C.1. POWER FLOW IN ROTOR FOR DIFFERENT ROTOR SPEEDS (ADAPTED FROM [C5])

Mode	Motor Subsynch	Motor Supersynch	Generator Supersynch	Generator Subsynch	Brake
Slip s	$0 < s < 1$	$s < 0$	$s < 0$	$0 < s < 1$	$s > 1$
Airgap power P_g	positive	positive	negative	negative	positive
Mechanical power P_m	positive	positive	negative	negative	negative
Slip power sP_g	positive	negative	positive	negative	positive

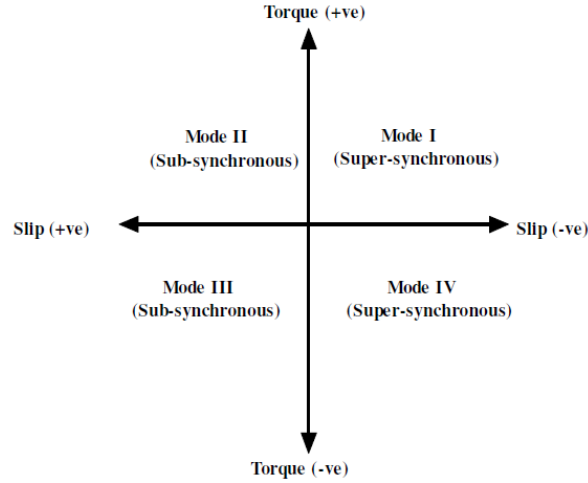


Fig. C.5. Different operating modes in a DFIG (adapted from [C7]).

The dynamic model of a DFIG is derived using two phase synchronous reference frame in which q-axis is 90^0 ahead of the d-axis with respect to the direction of rotation. The equivalent circuit of the DFIG in the dq synchronous reference frame is shown in Fig. C.6.

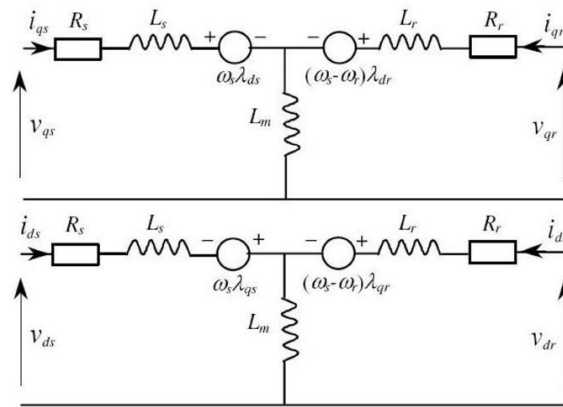


Fig. C.6. The equivalent circuit of a DFIG in the synchronous reference frame.

The DFIG model equations can be written as follows [C9].

$$v_{qs} = R_s i_{qs} + \omega_s \lambda_{ds} + \frac{d\lambda_{qs}}{dt} \quad (C.4)$$

$$v_{ds} = R_s i_{ds} - \omega_s \lambda_{qs} + \frac{d\lambda_{ds}}{dt} \quad (C.5)$$

$$v_{qr} = R_r i_{qr} + (\omega_s - \omega_r) \lambda_{dr} + \frac{d\lambda_{qr}}{dt} \quad (C.6)$$

$$v_{dr} = R_r i_{dr} - (\omega_s - \omega_r) \lambda_{qr} + \frac{d\lambda_{dr}}{dt} \quad (C.7)$$

$$\lambda_{qs} = L_{ls} i_{qs} + L_m (i_{qs} + i_{qr}) \quad (C.8)$$

$$\lambda_{ds} = L_{ls}i_{ds} + L_m(i_{ds} + i_{dr}) \quad (\text{C.9})$$

$$\lambda_{qr} = L_{lr}i_{qr} + L_m(i_{qs} + i_{qr}) \quad (\text{C.10})$$

$$\lambda_{dr} = L_{lr}i_{dr} + L_m(i_{ds} + i_{dr}) \quad (\text{C.11})$$

where the different symbols denote

v_{ds}, v_{qs} = Stator d and q winding voltages

v_{dr}, v_{qr} = Rotor d and q winding voltages

i_{ds}, i_{qs} = Stator d and q currents

i_{dr}, i_{qr} = Rotor d and q currents

$\lambda_{ds}, \lambda_{qs}$ = Stator d and q flux linkage

$\lambda_{dr}, \lambda_{qr}$ = Rotor d and q flux linkage

L_m = Magnetizing inductance

L_s, L_r = Stator and rotor per phase winding inductance

L_{ls}, L_{lr} = Stator and rotor per phase leakage inductance

R_s, R_r = Stator and rotor per phase winding resistance

ω_s, ω_r = synchronous speed and rotor speed

The active and reactive power transmitted through the stator or the rotor can be calculated using

$$P = \frac{3}{2}(v_q i_q + v_d i_d) \quad (\text{C.12})$$

$$Q = \frac{3}{2}(v_q i_d - v_d i_q) \quad (\text{C.13})$$

Different control strategies have been presented to control the back-to-back converters and maximum power point tracking in a DFIG [C1-C4, C7-C9, C11-C17]. Most common control techniques are associated with pulse width modulation (PWM) performing the active and reactive power control of DFIG separately. However, space vector pulse width modulation (SVPWM) has advantages with compared to usual PWM due to its simple digital implementation and higher modulation index [C10]. The conventional DFIG control system consists of d-q decoupling vector control of the rotor current [C3]. The d-q reference frame is usually aligned with either stator voltage vector or stator flux vector. The stator flux can be calculated by integrating the stator voltage.

(i) DFIG Model in PSCAD

Using the dynamic equations and dq reference frame transformation, a DFIG has been modeled for the simulation in PSCAD. The back-to-back three phase converter model used in simulation is shown in Fig. C.7. In the model developed, the GSC is responsible to maintain the DC link voltage constant irrespective of the magnitude and the direction of the rotor power. The control has been performed by aligning the reference frame with grid voltage vector. In this case, the d-axis current control the DC link voltage while q-axis current regulate the reactive power. The control blocks used to calculate the dq currents and dq voltages for GSC control are shown in Figs. C.8 and C.9 respectively. Moreover, the calculation of reference voltages for PWM generation and generation of firing pulses for

GSC switches are shown in Figs. C.10 and C.11 respectively. In the developed model in PSCAD, the RSC is responsible for controlling the bi-directional power flow through the converter. In this case, the q-axis current control the reactive power flow while d-axis current control the active power through the converter. The parameters of the DFIG model used in PSCAD are given in Table C.2 and Table C.3.

TABLE C.2 WIND TURBINE PARAMETERS

Parameter	Value
Rotor radius (m)	2.24
Maximum power coefficient	0.5
Optimal tip-speed ratio	10.9091
Base wind speed(m/s)	12 Hz
Maximum output power at base speed, $P_{o,base}$ (p.u.)	0.63
Generator speed at $P_{o,base}$ (p.u.)	1.1
Turbine torque at $P_{o,base}$ (p.u.)	0.76

TABLE C.3 WOUND ROTOR INDUCTION GENERATOR PARAMETERS

Parameter	Value
Rated power	12 kW
Rated voltage	0.415 V
Rated frequency	50 Hz
Stator resistance (p.u.)	0.06797
Stator leakage inductance(p.u.)	0.09225
Rotor resistance (p.u.)	0.05765
Rotor leakage inductance (p.u.)	0.09225
Magnetizing inductance (p.u.)	1.61455
The system moment of inertia (s)	3.694

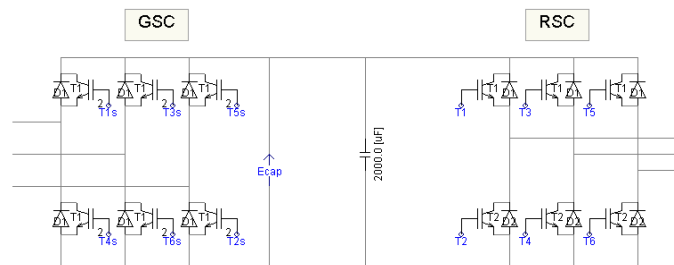


Fig. C.7. Back-to-back converter model in PSCAD.

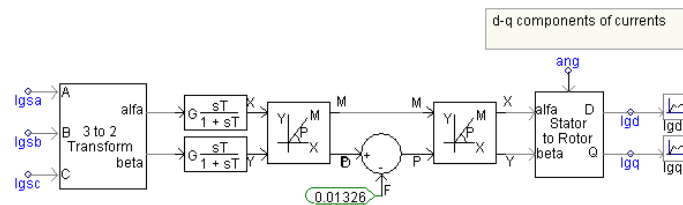


Fig. C.8. Calculation of dq currents for GSC control in PSCAD.

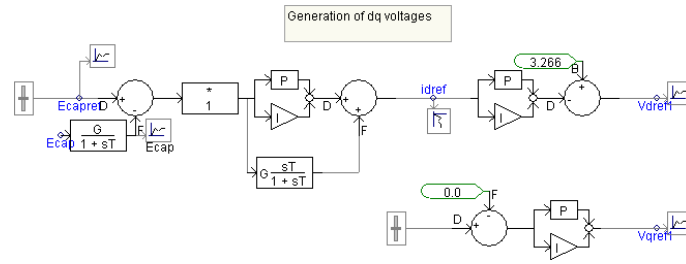


Fig. C.9. Calculation of dq voltages for GSC control in PSCAD.

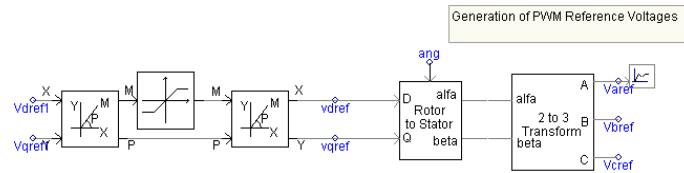


Fig. C.10. Calculation of reference voltages for PWM generation in PSCAD.

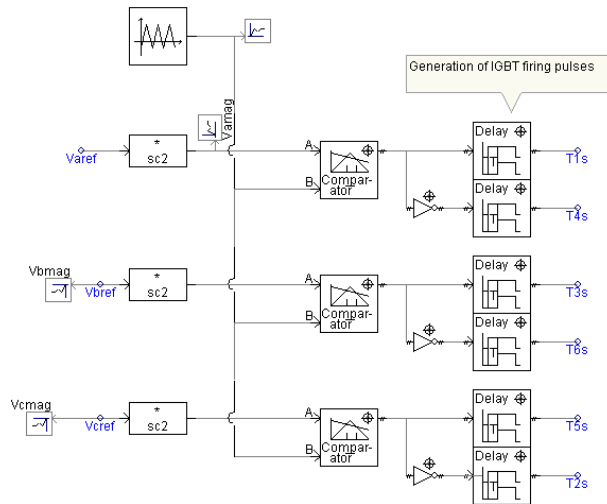


Fig. C.11. Generation of firing pulses for GSC in PSCAD.

(ii) DFIG Simulation Results

A DFIG connected to the utility grid as shown in Fig. C.12 is considered for the simulation. The parameters of the system are given in Table C.4.

TABLE C.5 SYSTEM PARAMETERS

System data	Value
System frequency	50 Hz
System voltage	0.415 kV rms (L-L)
Feeder impedance (Z_{l2})	$(0.0833 + j 0.8357) \Omega$
Load impedance ($load1=load2$)	$(15 + j 11.781) \Omega$

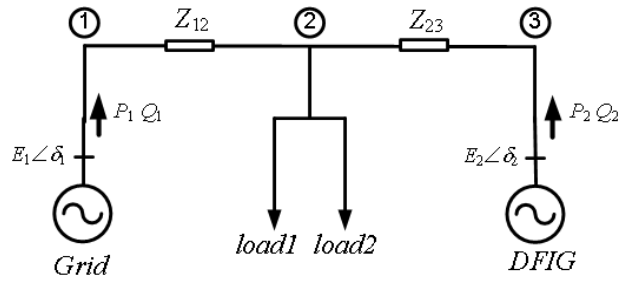


Fig. C.12. A DFIG connected to the grid.

It is assumed that the DFIG is connected to the grid and supplying the power in MPPT. The reactive power output of the DFIG is set to inject 2 kvar. Moreover, it is assumed that *load1* and *load2* are connected at the beginning and *load2* is disconnected at 8 s. The inertial wind speed for the DFIG is 12 m/s. However, the wind speed has changed gradually from 12m/s to 13m/s between 12 s and 14 s. The variation of real and reactive power output of the DFIG and the grid is shown in Fig. C.13. It can be seen that DFIG increases its real power output gradually while supplying the same reactive power into the system. The voltage waveform at PC of the DFIG and the output current of the DFIG are shown in Figs. C.14 and C.15 respectively. These results verify the DFIG model for further microgrid studies.

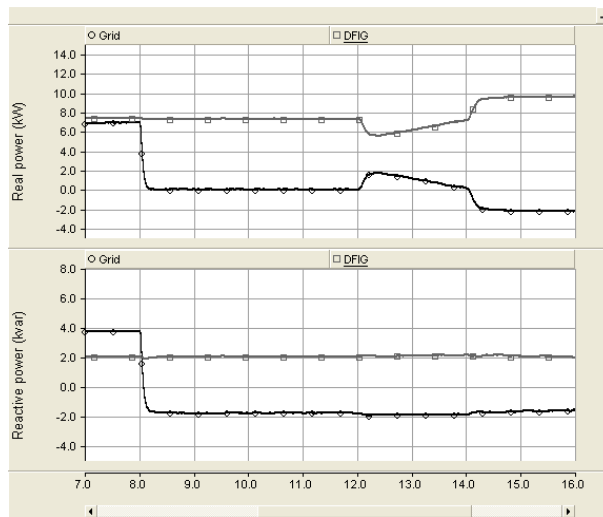


Fig. C.13. The variation of real and reactive power.

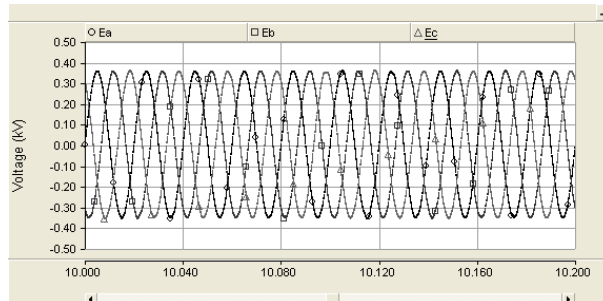


Fig. C.14. Voltage at PC of the DFIG.

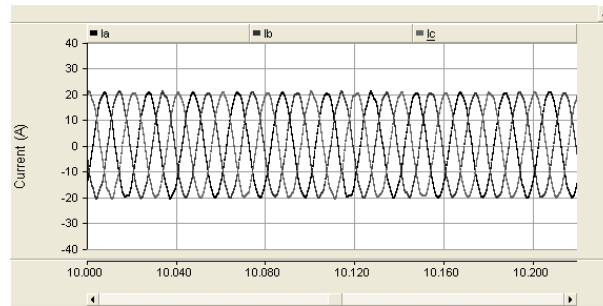


Fig. C.15. Output current of the DFIG

References

- [C1] J. Ning, W. Gao and J. Ojo, "Decoupled Control of Doubly Fed Induction Generator for Wind Power System," *The 40th North American Power Symposium*, 2008.
- [C2] M. Yin, G. Li, M. Zhou, G. Liu, and C. Zhao, "Study on the control of DFIG and its responses to grid disturbances," *IEEE Power Engineering Society General Meeting*, 2006.
- [C3] L. Xu and P. Cartwright, "Direct Active and Reactive Power Control of DFIG for Wind Energy Generation," *IEEE Transactions on Energy Conversion*, vol. 21, pp. 750-758, 2006.
- [C4] A. Tapia, G. Tapia, J. X. Ostolaza, and J. R. Saenz, "Modeling and Control of a Wind Turbine Driven Doubly Fed Induction Generator " *IEEE Transactions on Energy Conversion*, vol. 18, pp. 194-204, 2003.
- [C5] M. A. H. Salehy and M. N. Eskander, "Sub-Synchronous Range of Operation for a Wind Driven Double-Fed Induction Generator," *Journal of Power Electronics*, vol. 10, pp. 72-78, 2010.
- [C6] H. Sun, *et al.*, "DFIG Wind Power Generation Based on Back-to-back PWM Converter," *International Conference on Mechatronics and Automation*, 2009.
- [C7] M. Aktarujjaman, M. E. Haque, K. M. Muttaqi, M. Negnevitsky, and G. Ledwich, "Control Dynamics of a Doubly Fed Induction Generator Under Sub- and Super-synchronous Modes of Operation," *IEEE Power and Energy Society General Meeting*, 2008.
- [C8] R. Pena, J. C. Clare and G. M. Asher, "Doubly Fed Induction Generator using Back-to-back PWM Converters and Its Application to Variable-speed Wind-energy Generation " *IEE Proceedings - Electric Power Applications*, vol. 143, pp. 231-241, 1996.
- [C9] R. Aghatehrani, L. Fan and R. Kavasseri, "Coordinated Reactive Power Control of DFIG Rotor and Grid Sides Converters," *Power & Energy Society General Meeting*, 2009.
- [C10] H. Karimi-Davijani, A. Sheikholeslami, R. Ahmadi, and H. Livani, "Active and Reactive Power Control of DFIG Using SVPWM Converter," *The 43rd International Universities Power Engineering Conference*, 2008.
- [C11] A. G. Abo-Khalil, D. C. Lee and J. I. Jang, "Control of Back-to-Back PWM Converters for DFIG Wind Turbine Systems under Unbalanced Grid Voltage," *IEEE International Symposium on Industrial Electronics*, 2007.
- [C12] J. B. Ekanayake, L. Holdsworth, X. G. Wu, and N. Jenkins, "Dynamic Modeling of Doubly Fed Induction Generator Wind Turbines," *IEEE Transactions on Power Systems*, vol. 18, 2003.
- [C13] S. Muller, M. Deicke and R. W. D. Doncker, "Doubly Fed Induction Generator Systems for Wind Turbines," *IEEE Industry Applications Magazine*, vol. 8, pp. 26-33, 2002.
- [C14] T. K. A. Brekken and N. Mohan, "Control of a Doubly Fed Induction Wind Generator Under Unbalanced Grid Voltage Conditions " *IEEE Transactions on Energy Conversion*, vol. 22, pp. 129-135, 2007.
- [C15] S. Li and T. A. Haskew, "Analysis of Decoupled d-q Vector Control in DFIG Back-to-Back PWM Converter," *IEEE Power Engineering Society General Meeting*, 2007.
- [C16] H. Li, Z. Chen and J. K. Pederson, "Optimal Power Control Strategy of Maximizing Wind Energy Tracking and Conversion for VSCF Doubly Fed Induction Generator System," *The 5th International Power Electronics and Motion Control Conference*, 2006.
- [C17] O. Anaya-Lara, F. M. Hughes, N. Jenkins, and G. Strbac, "Rotor Flux Magnitude and Angle Control Strategy for Doubly Fed Induction Generators," *Wind Energ.* vol. 9, pp. 479-495, 2006.

Appendix-D: Photovoltaic Modeling

(i) PV Equivalent Circuit

A photovoltaic (PV) array consists with several solar cells connected with combination of series and parallel connections. Basically a solar cell is a p-n semiconductor junction which generates dc current when it exposes to sun light. The current generated depends on the solar irradiation and operating temperature. The equivalent circuit of a PV cell is shown in Fig. D.1.

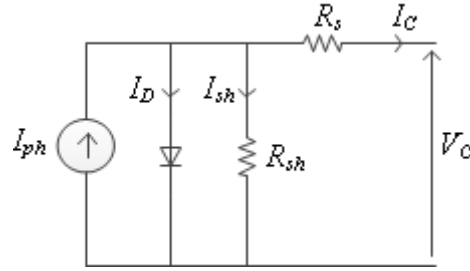


Fig. D.1. The equivalent circuit of a PV cell.

The I-V characteristic of a solar cell can be expressed as [D1, D2],

$$I_c = I_{ph} - I_d \times \left\{ \exp\left(\frac{q(V_c + I_c R_s)}{AkT_c}\right) - 1 \right\} \quad (D.1)$$

where the various symbols denote

- q =electron charge (1.602×10^{-19} C)
- k =Boltzman constant (1.38×10^{-23} J/K)
- I_c =cell output current (A)
- I_{ph} =photocurrent (A)
- I_d =Reverse saturation current of diode (A)
- R_s =series resistance of a cell
- T_c =Reference cell operating temperature (K)
- V_c =cell output voltage (V)

The value of shunt resistance is usually high and hence its effect has been neglected deriving the (D.1). The constant A is the curve fitting factor which is selected based on the I-V characteristic obtained from the testing. The short circuit current of a solar cell is obtained using (D.1) by substituting $V_c=0$. Output voltage of a PV cell can be expressed using (D.1) as

$$V_c = \frac{AkT_c}{q} \ln\left(\frac{I_{ph} - I_d - I_c}{I_d}\right) - R_s I_c \quad (D.2)$$

Similar to the short circuit current, the open circuit voltage of the solar cell is obtained by substituting $I_c=0$ in (D.2). Since $I_c \gg I_d$, the open circuit voltage can be approximated to

$$V_{oc} = \frac{AkT_c}{q} \ln \left(\frac{I_{ph}}{I_d} \right) \quad (D.3)$$

Total array voltage is calculated by multiplying the number of series connected cells with (D.2). The cell output current (i.e. I_C in (D.1)) is obtained by dividing the total array output current by the number of parallel PV cells connected. Output voltage and photocurrent of a cell change with operating temperature. However, the cell operating temperature changes with the ambient temperature and solar irradiation level. Thus there is a need to incorporate these changes in the PV array model.

The model in (D.1) is the bench mark model for known operating temperature (T_C) and known solar irradiation (S_C) level. Then the effect of different temperature and solar irradiation levels on photocurrent is incorporated to the model. It can be then expressed as [D3]

$$I_{ph} = I_{sc} \times \left[\frac{S}{S_{ref}} + C_T (T - T_{ref}) \right] \quad (D.4)$$

where I_{sc} is the short circuit current at reference temperature T_{ref} , S_{ref} is the reference solar irradiation level (i.e. usually 1000W/m²), C_T is the temperature coefficient for short circuit current. Similarly, using the temperature coefficient for open circuit voltage, the output voltage of the solar cell can be calculated. The temperature coefficient for short circuit is positive while it negative for open circuit voltage. So with the increase of temperature, short circuit current increases and open circuit voltage decreases.

Also the change of diode saturation current I_d with temperature can be given as [D2, D4]

$$I_d = I_{d,ref} \times \left[\frac{T}{T_{ref}} \right]^3 \times \exp \left\{ \frac{qE_g}{Ak} \left(\frac{1}{T_{ref}} - \frac{1}{T} \right) \right\} \quad (D.5)$$

$I_{d,ref}$ is the diode saturation current at reference temperature T_{ref} , T is the new temperature, E_g is the energy gap.

(ii) Maximum Power Point Tracking (MMPT) in PVs

The output power of photovoltaic cells shows a nonlinear characteristic depending on the solar irradiation level and temperature [D2, D6]. So the maximum power point varies with the changing atmospheric conditions. The variation of power with voltage for a typical PV array is shown in Fig. D.2.

In order to extract the maximum power continuously with the changes of atmospheric conditions it is necessary to track the maximum power from a solar array. In order to perform maximum power point tracking (MPPT), different controls have been proposed [D2, D6-D8]. The purpose of these MPPT is to move the operating voltage of PV array depending on the atmospheric conditions to extract the maximum power out of the array. The most popular MPPT techniques include perturbation and observation, incremental conductance, variable

incremental conductance, open circuit voltage, short circuit current, fuzzy logic controls and genetic algorithm. Each MPPT technique has advantages and disadvantages in implementation due to accuracy, complexity and cost of the control circuit involved. Some of the abovementioned MPPT control methods are briefly explained below.

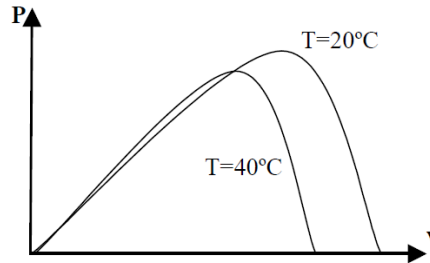


Fig. D.2. P-V characteristics at different temperatures

(a) MPPT based on Open Circuit Voltage Measurement

This is a simple method based on the observation that the ratio between array voltage at maximum power point tracking (V_{MPPT}) and array open circuit voltage (V_{OC}) is nearly a constant [D8].

$$V_{MPPT} = k_1 V_{OC} \quad (D.6)$$

The constant k_1 is reported to be 0.71 and 0.78. The array open circuit voltage V_{OC} is frequently measured to adjust the array output voltage based on k_1 . However, in this method the tracking accuracy and efficiency is relatively low due to the inaccurate assignment of constant k_1 .

(b) MPPT Based on the Short Circuit Current Measurement

This method is based on the ratio between the output current of a solar array at MPPT (i.e. I_{MPPT}) and short circuit current (I_{SC}) of the solar array is a constant [D6, D8].

$$I_{MPPT} = k_2 I_{SC} \quad (D.7)$$

The output current of a solar array is adjusted based on the measured short circuit current based on the constant k_2 . The values of constant k_2 are found to be between 0.78 and 0.92. The accuracy will depend on the accuracy of chosen value for k_2 and the measurement of short circuit current. A current transducer is required to measure the short circuit current periodically. However, two terminals of a PV array should be connected for taking the short circuit current measurement which can disturb the PV array performance. This method can track the MPPT very quickly even irradiation level changes rapidly.

(c) MPPT based on Perturbation and Observation (P&O)

This method is widely used in MPPT due to its simplicity and easy implementation. However, there are some drawbacks associated such as slow response speed, oscillation around MPPT in steady state [D9]. In this method, MPPT algorithm periodically increases or decreases the operating array voltage and monitors the output power change (ΔP) of PV array

[D1, D8]. Power voltage curve of a PV array has a global maximum at the MPPT. If the solar irradiation level is constant, for a given voltage perturbation, and if output power increases, then the next perturbation is generated in the same direction. Accordingly, operating point of PV array moves towards MPPT. Once it reaches the MPPT, the operating point oscillates around MPPT in steady state. However, if solar irradiation level has decreased suddenly, it may result in power decrease (negative ΔP) for perturbation in voltage change. This can lead to fail the tracking of MPPT [D6].

The change of voltage based on the MPPT algorithm is adjusted controlling the duty ratio of the switch in the DC chopper to achieve the maximum power point by repeating the process. In this case, the system oscillates around the MPPT as mentioned. These oscillations can be minimized by using a small step change. However, it may slow down the process of MPPT.

(d) MPPT based on Incremental conductance

This method is based on the slope of the PV array power curve. Once maximum power point reaches, the slope should be zero [D8]. Thus, the MPPT controller judges whether a PV array operates left or right side to the MPPT and the adjustments to the array output voltage are made accordingly till the condition for maximum power tracking is satisfied. The performance of tracking can be improved by using a variable step incremental conductance method [D10].

To implement the MPPT algorithm in a solar array, a control circuit is necessary. Usually a DC-DC circuit (i.e. buck, boost or buck-boost) is used to accomplish the MPPT by controlling the duty ratio of the switch [D1]. In [D6], boost converter is used. The boost converter is a good choice for MPPT since they have simple structure and control, and high efficiency [D10].

(iii) Solar Cell Characteristic Obtained from MATLAB

In this section, above explained PV array characteristics are obtained using MATLAB calculations. For this purpose, a solar panel module is considered and parameters are given in Table D.1. The current voltage (I-V) characteristics of the solar module for different temperature values and different solar irradiation levels are shown in Figs. D.3 and D.4. As can be seen from the figures, the open circuit voltage reduces when the operating temperature increases while the short circuit current reduces when the solar irradiation level decreases. The power voltage (P-V) characteristics of the selected solar array are shown in Figs. D.5 and D.6. It can be seen that the output power decreases when the operating temperature increases and the solar irradiation level reduces. However, one of the MPPT methods mentioned above can be used to extract the maximum available power from the solar module depending on the temperature and solar irradiation level.

TABLE D.1 PV SOLAR PARAMETERS

Parameter	Value
Max. peak power (MPP)	170 W
Voltage at MPP	35.7 V
Current at MPP	4.9 A
Open circuit voltage	44.5 V
Short circuit current	5.21 A

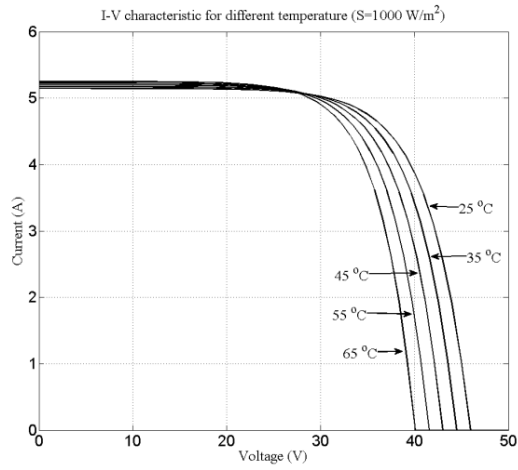


Fig. D.3. I-V characteristics of PV for different temperature.

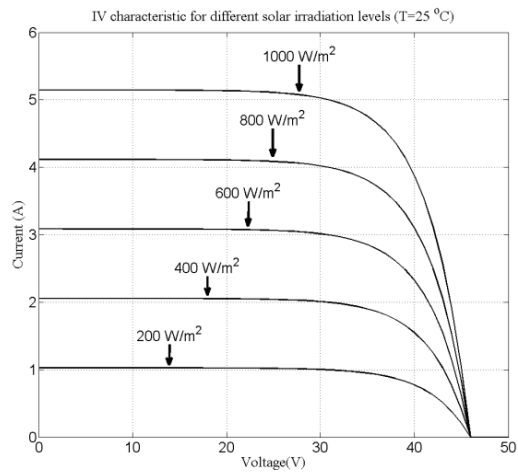


Fig. D.4. I-V characteristics of PV for different solar irradiation levels.

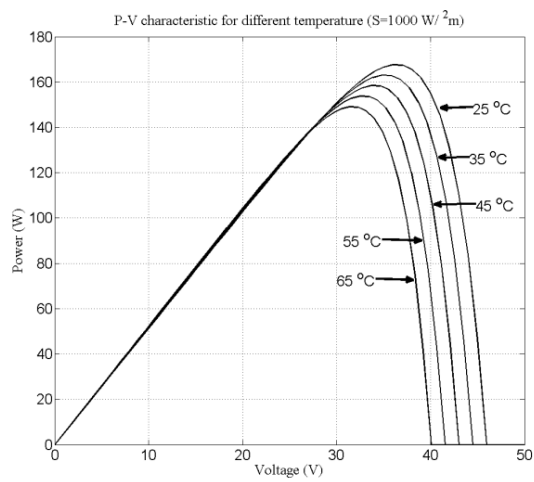


Fig. D.5. P-V characteristics of PV for different temperature.

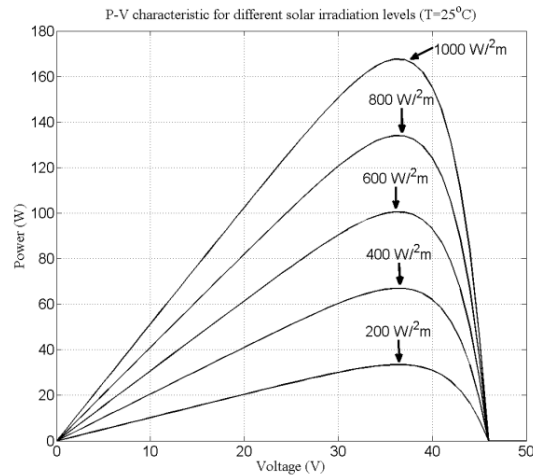


Fig. D.6. P-V characteristics of PV for different solar irradiation levels.

References

- [D1] C. Hua and C. Shen, "Study of maximum power tracking techniques and control of DC/DC converters for photovoltaic power system," *29th Annual IEEE Power Electronics Specialists Conference*, pp. 86 - 93, 1998.
- [D2] Y. Chuanan and Y. Yongchang, "An Improved Hill-Climbing Method for the Maximum Power Point Tracking in Photovoltaic System," *IEEE International Conference on Machine Vision and Human-Machine Interface*, pp. 530 - 533 2010.
- [D3] S.-K. Kim, J.-H. Jeon, C.-H. Cho, E.-S. Kim, and J.-B. Ahn, "Modeling and simulation of a grid-connected PV generation system for electromagnetic transient analysis," *Solar Energy*, vol. 83, pp. 664-678, 2009.
- [D4] J. Xue, Z. Yin, B. Wu, and J. Peng, "Design of PV Array Model Based On EMTDC/PSCAD," *Power and Energy Engineering Conference*, pp. pp.1-5, 2009.
- [D5] I. H. Altas and A. M. Sharaf, "A Novel Photovoltaic On-Line Search Algorithm For Maximum Energy Utilization," *The International Conference on Communication, Computer and Power* 2007.
- [D6] C. Zhang, D. Zhao, J. Wang, Y. An, and G. Chen, "A novel two-mode MPPT method for photovoltaic power generation system," *IEEE 6th International Power Electronics and Motion Control Conference* pp. 2100 - 2102 2009.
- [D7] S. Jain and V. Agarwal, "A new algorithm for rapid tracking of approximate maximum power point in photovoltaic systems," *IEEE Power Electronics Letters*, vol. 2, pp. 16 - 19 2004.
- [D8] M. Azab, "A New Maximum Power Point Tracking for Photovoltaic Systems," *Proceedings of World Academy of Science, Engineering and Technology*, vol. 34, pp. 571-574, 2008.
- [D9] X. Liu and L. A. C. Lopes, "An improved perturbation and observation maximum power point tracking algorithm for PV arrays," *IEEE 35th Annual Power Electronics Specialists Conference*, vol. 3, pp. 2005 - 2010, 2004.
- [D10] H. Zhang, H. Ji, J. Ren, L. Shan, and Y. Gao, "Research on MPPT control and implementation method for photovoltaic generation system and its simulation," *IEEE 6th International Power Electronics and Motion Control Conference* pp. 2108 - 2112 2009.